Article

A genome-scale screen for synthetic drivers of T cell proliferation

https://doi.org/10.1038/s41586-022-04494-7

Received: 2 June 2021

Accepted: 1 February 2022

Published online: 16 March 2022

Check for updates

Mateusz Legut[1,2,3,4]✉, Zoran Gajic[1,2,3,4], Maria Guarino[1,2,3,4], Zharko Daniloski[1,2,3,4,7], Jahan A. Rahman[1,2,3,4], Xinhe Xue[1,2,3,4], Congyi Lu[1,2,3,4], Lu Lu[1,2,3,4], Eleni P. Mimitou[5,8], Stephanie Hao[5], Teresa Davoli[4,6], Catherine Diefenbach[4], Peter Smibert[5,8] & Neville E. Sanjana[1,2,3,4]✉

The engineering of autologous patient T cells for adoptive cell therapies has revolutionized the treatment of several types of cancer[1]. However, further improvements are needed to increase response and cure rates. CRISPR-based loss-of-function screens have been limited to negative regulators of T cell functions[2–4] and raise safety concerns owing to the permanent modification of the genome. Here we identify positive regulators of T cell functions through overexpression of around 12,000 barcoded human open reading frames (ORFs). The top-ranked genes increased the proliferation and activation of primary human CD4$^+$ and CD8$^+$ T cells and their secretion of key cytokines such as interleukin-2 and interferon-γ. In addition, we developed the single-cell genomics method OverCITE-seq for high-throughput quantification of the transcriptome and surface antigens in ORF-engineered T cells. The top-ranked ORF—lymphotoxin-β receptor (LTBR)—is typically expressed in myeloid cells but absent in lymphocytes. When overexpressed in T cells, LTBR induced profound transcriptional and epigenomic remodelling, leading to increased T cell effector functions and resistance to exhaustion in chronic stimulation settings through constitutive activation of the canonical NF-κB pathway. *LTBR* and other highly ranked genes improved the antigen-specific responses of chimeric antigen receptor T cells and γδ T cells, highlighting their potential for future cancer-agnostic therapies[5]. Our results provide several strategies for improving next-generation T cell therapies by the induction of synthetic cell programmes.

Cellular immunotherapies with engineered autologous patient T cells redirected against a chosen tumour antigen have yielded great efficacy against blood cancers, resulting in five approvals for chimeric antigen receptors (CARs) by the US Food and Drug Administration (FDA) so far[6]. By contrast, CAR therapy for solid tumours has shown a much lower efficacy overall, owing to the suppression of T cell effector function in the tumour microenvironment. Even for blood malignancies, with the exception of B acute lymphoblastic leukaemia, most patients do not experience a durable response, with resistance being primarily due to T cell dysfunction rather than antigen loss[7]. Considerable efforts have been devoted to identifying genes and pathways that contribute to T cell dysfunction[8,9]. However, comprehensive, genome-wide screens for modulators of T cell function thus far have been limited to loss-of-function screens[2–4].

The advances in CRISPR genome engineering have made it possible to readily knock out every gene in the genome in a scalable and customizable manner. Although its large size makes it challenging (albeit not impossible[10]) to deliver Cas9 via lentivirus to primary T cells, alternative approaches have been developed, which rely on transient delivery of Cas9 protein[2] or mRNA[11], or on constitutive Cas9 expression in engineered isogenic mouse strains[3]. These approaches, however, are not amenable to gain-of-function screens in human cells, which require continuous expression of the transcriptional activator that drives target gene expression. The large size and immunogenicity of most Cas9–transcriptional activator fusion proteins have limited their use in T cell engineering for in vivo or clinical approaches[12].

Here we perform a genome-scale gain-of-function screen in primary human CD4$^+$ and CD8$^+$ T cells, using a lentiviral library of barcoded human ORFs. We show that T cells with the strongest proliferation phenotypes are enriched for both known and unknown regulators of the immune response, many of which are not typically expressed by peripheral T cells. We validate top-ranked ORFs in cells from screen-independent donors and further demonstrate that these ORFs not only drive T cell proliferation but also increase the expression of activation markers and the secretion of key proinflammatory cytokines. To gain more comprehensive insight into the mechanism of action of these genes, we develop a single-cell sequencing approach coupled with direct ORF capture. We identify LTBR—one of the top-ranked ORFs not expressed by lymphocytes—as a key driver of profound transcriptional and epigenetic remodelling through increased NF-κB signalling,

[1]New York Genome Center, New York, NY, USA. [2]Department of Biology, New York University, New York, NY, USA. [3]Department of Neuroscience and Physiology, New York University School of Medicine, New York, NY, USA. [4]Perlmutter Cancer Center, New York University School of Medicine, New York, NY, USA. [5]Technology Innovation Lab, New York Genome Center, New York, NY, USA. [6]Department of Biochemistry and Molecular Pharmacology, New York University School of Medicine, New York, NY, USA. [7]Present address: Beam Tx, Cambridge, MA, USA. [8]Present address: Immunai, New York, NY, USA. ✉e-mail: mateusz.legut@gmail.com; neville@sanjanalab.org

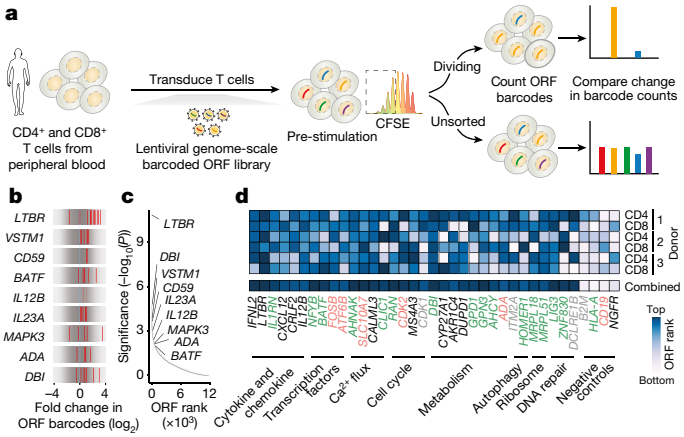

Fig. 1 | A genome-scale overexpression screen to identify genes that boost the proliferation of primary human T cells. a, Overview of the pooled ORF screen. CD4$^+$ and CD8$^+$ T cells were separately isolated from peripheral blood from three healthy donors. The barcoded genome-scale ORF library was then introduced into CD3/CD28-stimulated T cells, followed by selection of transduced cells. After 14 days of culture, T cells were labelled with carboxyfluorescein succinimidyl ester (CFSE) and restimulated to induce proliferation. By comparing counts of specific ORF barcodes before and after cell sorting, we identified ORFs enriched in the CFSE^{low} population. **b**, Normalized enrichment of individual barcodes for the indicated genes in the CD4$^+$ screen. **c**, Robust rank aggregation of genes in both CFSE^{low}CD4$^+$ and CFSE^{low}CD8$^+$ T cells, based on consistent enrichment of individual barcodes for each gene. **d**, Enrichment in individual donors and T cell populations of top-ranked genes (grouped by function and relevance to T cell proliferation) selected for further study. Neutral genes (MHC-I complex and cell-type-specific differentiation markers) are included for comparison. Gene names are coloured on the basis of the differential expression in CD3/CD28-stimulated and resting T cells (green, upregulated; red, downregulated; grey, no change; black, no expression)[41].

which results in a marked increase in the secretion of proinflammatory cytokines and resistance to apoptosis. Finally, we show that top-ranked ORFs potentiate antigen-specific T cell functions, in the context of CD19-directed CAR T cells and broadly tumour-reactive γδ T cells from healthy donors and patients with blood cancer.

Genome-scale ORF screen in T cells

To avoid relying on constitutive expression of large bacterial proteins or chromatin accessibility in the vicinity of target genes[13], we decided to use a lentiviral library of human ORFs; this library contains nearly 12,000 full-length genes, with around 6 barcodes per gene[14] (Fig. 1a, Extended Data Fig. 1a–g). Previously, genome-scale loss-of-function screens in human T cells have focused on either CD4$^+$ or CD8$^+$ T cells. However, both CD4$^+$ and CD8$^+$ T cells are required for durable tumour control in adoptive therapies[15,16], as further exemplified by FDA approvals of anti-CD19 CAR T cells with a defined 1:1 CD4$^+$ and CD8$^+$ ratio[1]. Thus, we decided to use the ORF library to discover genes that boost the proliferation of both CD4$^+$ and CD8$^+$ T cells in response to T cell receptor (TCR) stimulation (Fig. 1a, Extended Data Fig. 1h–j).

We transduced the lentiviral ORF library into CD4$^+$ and CD8$^+$ T cells from three healthy donors, and after a brief period in culture (14 days) we restimulated the cells to identify drivers of proliferation in response to TCR stimulation. We were able to capture the majority of individual ORF barcodes, and nearly all ORFs, including the largest ones (Extended Data Fig. 1k, l). Comparing the relative frequencies of genes in the most highly proliferative cells to unsorted cells, we found an enrichment of genes that are known to participate in immune processes among the top-ranked ORFs (Extended Data Fig. 1m, n). We identified *MAPK3* (encoding ERK1), a critical mediator of T cell functions[17], the co-stimulatory molecule CD59[18], the transcription factor BATF, and cytokines that are known to promote T cell proliferation, such as IL12B and IL23A[19]. In fact, two recent studies showed that overexpression of IL12B and BATF boosts proliferation, cytotoxicity and cytokine secretion in CAR T cells[19,20].

Each ORF in the library is linked to an average of six DNA barcodes (Extended Data Fig. 1b). To increase confidence in our top-ranked ORFs from the pooled screen, we assessed the enrichment of individual barcodes corresponding to a given ORF in proliferating CD4$^+$ and CD8$^+$ cells (Fig. 1b, c, Extended Data Fig. 1o). For the majority of ORFs, multiple individual barcodes for each gene were enriched in the highly proliferating population, thus suggesting that the observed enrichment does not stem from spurious clonal outgrowth or PCR bias. Surprisingly, the most significantly enriched gene was lymphotoxin-β receptor (*LTBR*), a gene that is broadly expressed in stromal and myeloid cells but completely absent in lymphocytes.

Overall, the enriched ORFs spanned a range of diverse biological processes. Among the top-enriched Gene Ontology (GO) biological processes were lymphocyte proliferation, interferon-γ (IFNγ) production and NF-κB signalling (Extended Data Fig. 1p). We observed that enriched ORFs showed only a slight preference for genes endogenously upregulated by T cells during stimulation with CD3 and CD28 (CD3/CD28), and in fact were represented in all classes of differential expression (Extended Data Fig. 1q). This result highlights the capacity of the pooled ORF screen to discover genes that enable T cell proliferation but that are not expressed normally during CD3/CD28-mediated activation and proliferation. For subsequent validation, we decided to test a broad range of ORFs that function in diverse pathways of relevance to T cell fitness, and that showed different modes of endogenous regulation (Fig. 1d).

Top ORFs enhance T cell functions

To validate the top-ranked ORFs and understand their effect on other relevant aspects of T cell function, we subcloned 33 ORFs from the library into a vector co-expressing a P2A-linked puromycin resistance gene from the same promoter. We chose a truncated nerve growth factor receptor (tNGFR), lacking its intracellular domain, as a control that has no effect on T cell phenotype[21]. CD4$^+$ and CD8$^+$ populations were separately isolated from several screen-independent healthy donors and transduced with individual ORFs (Fig. 2a). Using flow cytometry on representative ORFs, we confirmed that they were stably and uniformly expressed in both subsets of T cells for the duration of the experiment (Extended Data Fig. 2a, b).

Fourteen days after isolation, we restimulated the cells and measured the relative increase in cell numbers. We found that 16 tested ORFs significantly improved cell proliferation compared with tNGFR, and that proliferation was well correlated between CD4$^+$ and CD8$^+$ cells (Spearman's $r = 0.61$, $P = 0.002$) (Fig. 2b, c, Extended Data Fig. 2c–h). Having established that the top ORFs improve T cell proliferation, we next tested whether there is also a change in other T cell phenotypes and functions, such as increased cell cycle entry, expression of the activation markers IL2RA (CD25) and CD40L (CD154), and cytokine secretion. Most of the ORFs tested showed no difference in cycling (Extended Data Fig. 2i, j), but showed higher expression of both CD25 and CD154 in T cells after stimulation (Fig. 2d, Extended Data Fig. 3a), further corroborating their effect in improving the magnitude of T cell responses.

Finally, we measured the secretion of the cytokines interleukin-2 (IL-2) and IFNγ after restimulation with CD3/CD28 (Fig. 2e, Extended Data Fig. 3b–e). Although our screen was not designed to identify genes that modulate cytokine secretion, several ORFs could both improve T cell proliferation and boost IL-2 or IFNγ secretion (Fig. 2f). The strongest effect was observed for LTBR, which increased the secretion of both these cytokines in CD4$^+$ and CD8$^+$ T cells by more than fivefold.

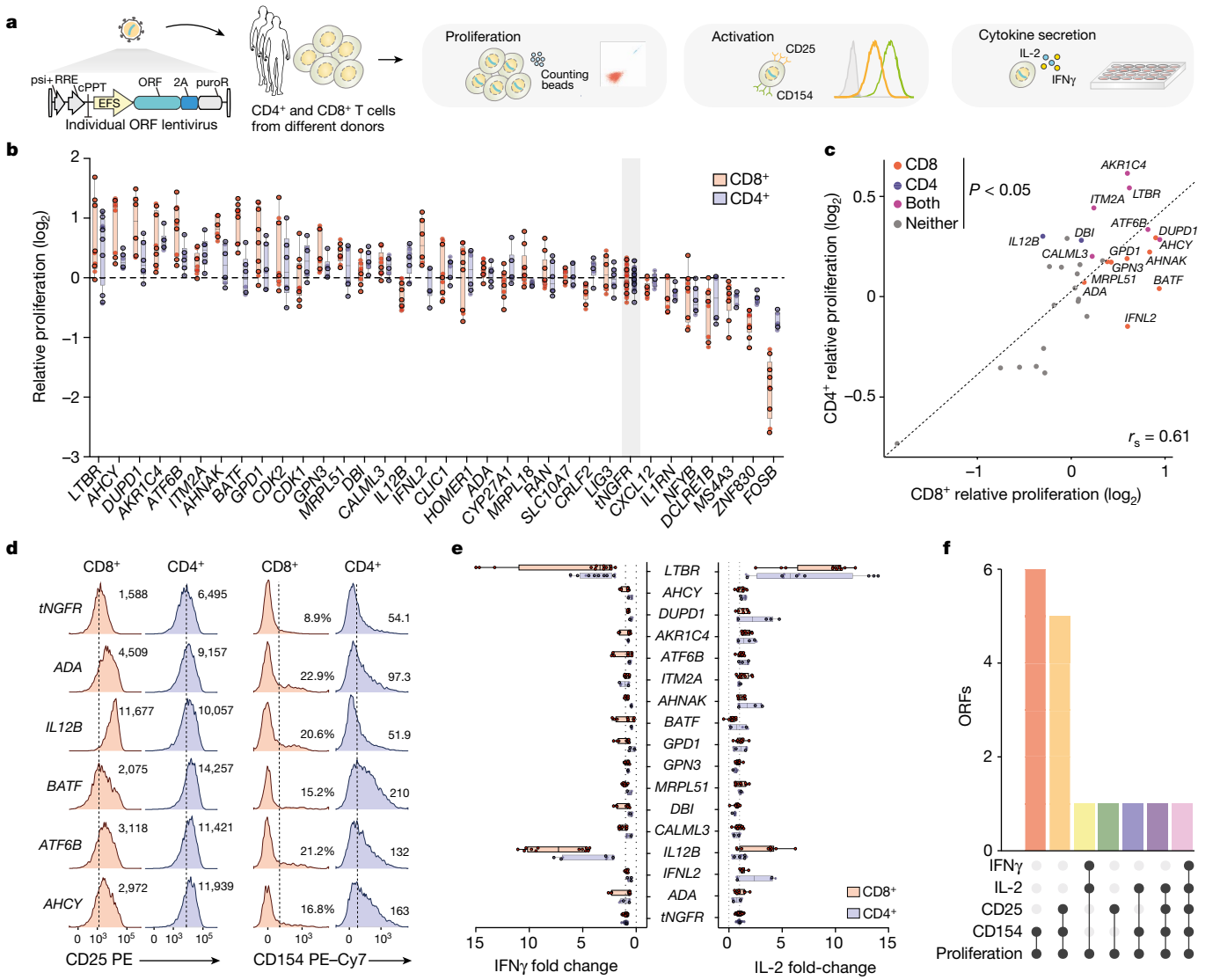

Fig. 2 | Overexpression of top-ranked ORFs increases the proliferation, activation and cytokine secretion of CD4$^+$ and CD8$^+$ T cells. a, CD4$^+$ and CD8$^+$ T cells from screen-independent donors were separately isolated and then transduced with lentiviruses encoding top-ranked ORFs together with a selection marker. After transduction and selection, T cells were restimulated before measurement of proliferation, expression of activation markers and cytokine secretion. **b**, Proliferation of T cells transduced with top-ranked genes as the relative proliferation, which is defined as the ratio of stimulated cells to the corresponding unstimulated control, normalized to tNGFR. A minimum of two donors was tested per overexpressed gene, in biological triplicate. Boxes show 25th–75th percentiles with a line at the mean; whiskers extend to maximum and minimum values. *DUPD1* is also known as *DUSP29*. **c**, Mean relative proliferation of ORF-transduced T cells in CD4$^+$ and CD8$^+$ T cells, normalized to tNGFR. Significant genes in both T cell subsets or either of them are marked (Student's two-sided *t* test $P < 0.05$ and false discovery rate < 0.1). **d**, Representative expression of CD25 or CD154 after restimulation. The numbers on the histograms correspond to the percentage of gated cells (CD8$^+$CD154$^+$) or the mean fluorescence intensity (MFI). Dashed lines indicate the gate used to enumerate CD154$^+$ cells (CD8$^+$) or MFI for control (tNGFR) cells. **e**, Secretion of IL-2 and IFNγ after restimulation, normalized to tNGFR. Only genes that significantly increase T cell proliferation in CD4$^+$, CD8$^+$ or both T cell subsets are shown. A minimum of two donors was tested in triplicate per gene. Boxes show 25th–75th percentiles with a line at the mean; whiskers extend to maximum and minimum values. **f**, Intersection between different T cell activation phenotypes that are significantly ($P < 0.05$) improved by a given ORF in CD8$^+$ or CD4$^+$ T cells. The mean $\log_2$-transformed fold change, two-sided *t* test *P* value and false discovery rate for each ORF and phenotype are shown in Supplementary Table 6.

Single-cell analysis of ORF phenotypes

Building on our quantification of how each ORF affects proliferation, activation and cytokine release, we next sought to better understand the underlying mechanisms that drive these changes in cell state. To gain a more comprehensive view of the mechanisms of action of individual ORFs, and to provide a multidimensional characterization of the phenotypic changes they induce, we developed a single-cell sequencing strategy with direct ORF capture. This approach, OverCITE-seq (Overexpression-compatible Cellular Indexing of Transcriptomes and Epitopes by Sequencing) extends previous approaches that we have developed for quantifying surface antigens[22] and CRISPR perturbations[23], and allows for high-throughput, single-cell analysis of a pool of T cells with different ORFs. In brief, mRNA from lentivirally integrated ORFs is reverse-transcribed by a primer binding to a constant sequence of the transcript downstream of the ORF and barcoded, along with the cell transcriptome, during template switching. The resulting cDNA pool is then split for separate construction of gene expression and ORF expression libraries (Fig. 3a, b, Extended Data Fig. 4a).

We optimized and applied OverCITE-seq to a pool of around 30 ORFs transduced into CD8$^+$ T cells from a healthy donor. The cell pool was either left unstimulated ('resting') or stimulated with CD3/CD28

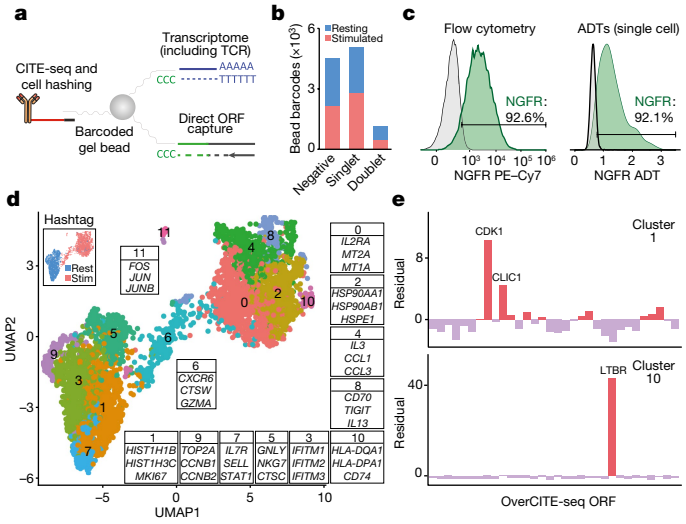

Fig. 3 | Single-cell OverCITE-seq identifies shared and distinct transcriptional programs that are induced by gene overexpression in T cells. a, OverCITE-seq captures overexpression (ORF) constructs, transcriptomes, TCR clonotypes, cell-surface proteins and treatment hashtags in single cells. **b**, ORF assignment rate in resting and CD3/CD28-stimulated T cells. **c**, Antibody-derived tag sequencing (ADTs; right) yields similar NGFR expression in tNGFR-transduced T cells to flow cytometry (left) with tNGFR-transduced T cells. Untransduced cells (left) or cells assigned a non-tNGFR ORF (right) are shown in grey. **d**, Uniform manifold approximation and projection (UMAP) representation of single-cell transcriptomes after unsupervised clustering of OverCITE-seq-captured ORF singlets. The inset in the top left identifies stimulated and resting T cells as given by treatment hashtags. For each cluster, a subset of the top 20 differentially expressed genes is shown. *HIST1H1B* is also known as *H1-5* and *HIST1H3C* is also known as *H3C3*. **e**, ORF prevalence in two representative clusters. Standardized residual values are from a chi-squared test. ORFs of interest are shown.

antibodies to mimic TCR activation. To gain confidence in how well ORFs are assigned to each single cell, we leveraged the fact that the protein produced by the control gene, tNGFR, is expressed on the cell surface and can thus be captured with a DNA-barcoded antibody[23]. The proportion of cells designated as tNGFR positive was consistent when measured by CITE-seq or flow cytometry (Fig. 3c). An analysis of the entire ORF pool showed that single cells assigned with a given ORF had overall the strongest expression of the corresponding gene (Extended Data Fig. 4b–d), indicating that our ORF capture strategy reliably assigned a genetic perturbation to each single cell.

Unsupervised clustering showed clear separation for stimulated and resting T cells. Within these activation-driven super-clusters we could observe individual clusters associated with a particular cell state or function, such as cell cycle (clusters 1 and 9), macromolecule biosynthesis (cluster 2), type I IFN signalling (cluster 3), cytotoxicity (cluster 6), T cell activation and proliferation (cluster 10), and stress response and apoptosis (cluster 11) (Fig. 3d). Although in many cases several ORFs contributed to a given cluster phenotype (Extended Data Fig. 4e), we observed a notable enrichment of two ORFs, CDK1 and CLIC1, in cluster 1, characterized by the increased expression of genes that are responsible for chromosome condensation in preparation for cell cycle (Fig. 3e). An even stronger enrichment was observed for cluster 10, which was almost exclusively composed of cells expressing LTBR.

To investigate the mechanisms of genetic perturbations with the strongest transcriptional changes, we looked at the transcriptomic profiles of CD3/CD28-stimulated ORF T cells compared to unstimulated control T cells (Extended Data Fig. 4f–i). This approach allowed us to identify gene modules that are shared between perturbations or that are perturbation-specific. For example, LTBR and CDK1 showed the strongest enrichment of genes involved in RNA metabolism and cell cycle (*CDK4*, *HSPA8* and *BTG3*), as well as in the tumour necrosis factor (TNF) signalling pathway (*TNFAIP3*, *TRAF1* and *CD70*). FOSB appeared to drive an opposite programme to LTBR in terms of genes involved in TCR signalling (*CD3D*, *CD3E*, *LAPTM5* and *LAT*), cytokine responses (*GATA3* and *TNFRSF4*) and the NF-κB pathway (*NFKB2*, *NFKBIA* and *UBE2N*). Finally, we determined that the observed phenotypes were a result of a genetic perturbation rather than an outgrowth of a single clone because virtually every single cell expressed a unique TCR clonotype (Extended Data Fig. 4j). This result highlights the utility of OverCITE-seq's multimodal capture approach, yielding each T cell's transcriptome, clonotype, cell surface proteome, cell hashing (for treatment or stimulation conditions) and lentiviral ORF identity.

LTBR improves multiple T cell functions

Having identified LTBR as a strong driver of proinflammatory cytokine secretion (Fig. 2e) and profound transcriptional remodelling (Fig. 3d, e), we decided to investigate its mechanisms of action in more detail. LTBR belongs to the tumour necrosis factor receptor superfamily (TNFRSF) and is expressed on a variety of non-immune cell types and on immune cells of myeloid origin, but is absent from lymphocytes (Extended Data Fig. 5a, b). Using bulk RNA sequencing (RNA-seq), we compared global gene expression between LTBR- and tNGFR-transduced cells, with or without TCR stimulation (Fig. 4a, b, Extended Data Fig. 5c). In addition to upregulation of MHC-I and II genes (*HLA-C*, *HLA-B*, *HLA-DPB1*, *HLA-DPA1* and *HLA-DRB6*) and transcription factors necessary for MHC-II expression (*RFX5* and *CIITA*), LTBR cells also expressed the MHC-II invariant chain (encoded by *CD74*). Notably, CD74 has been shown in B cells to activate the pro-survival NF-κB pathway, in particular through upregulation of the anti-apoptotic genes *TRAF1* and *BIRC3* (both of which are also upregulated in LTBR-overexpressing cells)[24]. Similarly, LTBR cells strongly upregulated *BATF3*, which has been shown to promote the survival of $CD8^+$ T cells[25]. We also observed upregulation of *JUNB*, a transcription factor involved in IL-2 production[26], and *TCF7* (encoding TCF1), a key transcription factor responsible for T cell self-renewal[27]. We confirmed the RNA-seq results at the protein level (Extended Data Fig. 5d–i). LTBR cells were also more resistant to activation-induced cell death and retained greater functionality after repeated stimulations (Fig. 4c, d, Extended Data Fig. 5j–m).

LTBR signalling in its endogenous context (in myeloid cells) is triggered either by a heterotrimer of lymphotoxin-α (LTA) and lymphotoxin-β (LTB) or by LIGHT (encoded by the *TNFSF14* gene). As LTA, LTB and LIGHT are expressed by activated T cells, we sought to elucidate whether addition of exogenous LTA or LIGHT could modulate the cytokine secretion, differentiation or proliferation of CD3/CD28-stimulated LTBR-overexpressing T cells; however, we found no effect of exogenous ligands on LTBR T cell function (Extended Data Fig. 6a–e). Thus, although LTBR could potentiate the TCR-driven T cell response, it does not drive activation on its own—which would be a potential safety issue and result in loss of antigen specificity of the engineered T cell response. We also determined that constitutive expression of LTBR is required for maintenance of its phenotype but that there is a substantial lag time between loss of detectable LTBR expression and loss of phenotype (Extended Data Fig. 6f–i), indicating that transient expression of LTBR may be a safe avenue into a therapeutic application.

Finally, to identify the key domains of the LTBR protein that drive its activity in T cells, we designed a series of point or deletion mutants of LTBR (Fig. 4e, Extended Data Fig. 6j). In general, we found that the N terminus of LTBR was less sensitive to deletions than the C terminus. Similarly, a partial reduction of the LTBR phenotype was achieved by introducing three alanine point mutations in the key residues for LTA and LTB binding[28], or by removal of the signal peptide. Using our C-terminal deletions, we found that a mutant version of LTBR that lacks residues 393–435 showed no difference compared with full-length

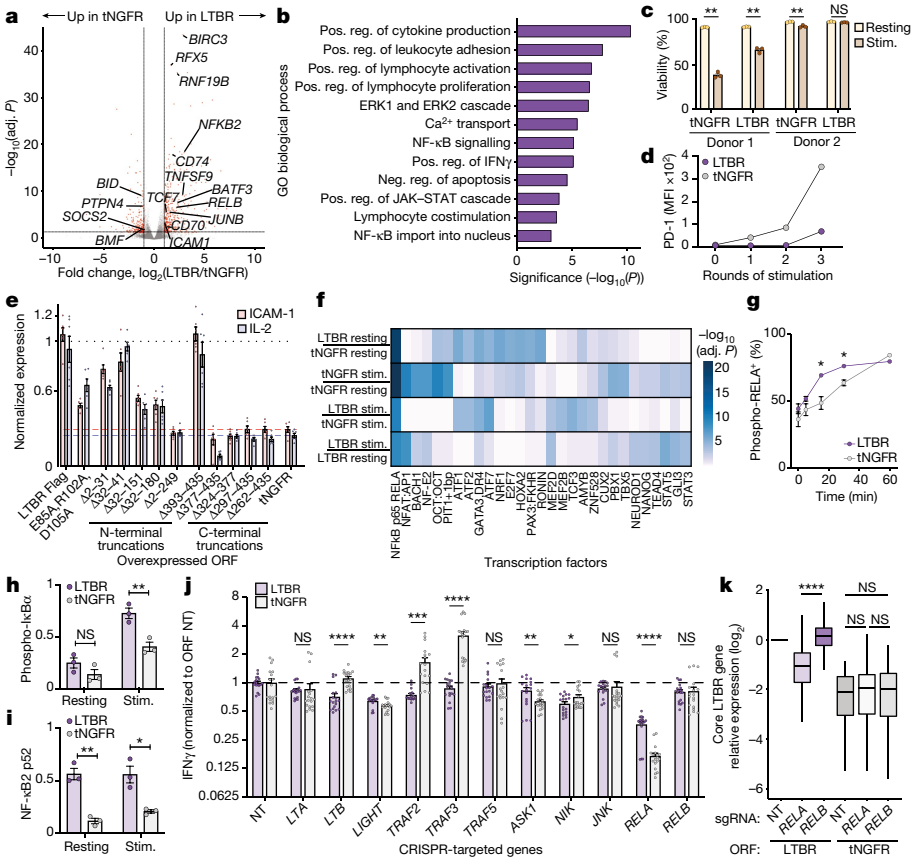

Fig. 4 | LTBR overexpression improves T cell function through activation of the canonical NF-κB pathway. a, Differential expression of genes in resting LTBR and tNGFR (negative control) T cells. Genes highlighted in red are those with a twofold or greater change in expression and an adjusted $P < 0.05$. **b**, Significantly enriched GO biological processes in LTBR-overexpressing T cells ($p < 0.05$). **c**, Cell viability of $CD8^+$ T cells transduced with LTBR or tNGFR lentivirus, either restimulated with CD3/CD28 for four days or left unstimulated ($n = 2$ donors with 3 biological replicates each). **d**, PD-1 expression on resting LTBR or tNGFR T cells stimulated with a 3:1 excess of CD3/CD28 beads every three days, for up to three rounds of consecutive stimulation. **e**, ICAM-1 expression (resting) and IL-2 secretion (activated) by T cells transduced with Flag-tagged LTBR mutants, normalized to wild-type LTBR ($n = 6$ replicates across two experiments). **f**, Enrichment of transcription factor motifs in differentially accessible chromatin (top 10 motifs from each comparison). **g**, Quantification of phosphorylated RELA (phospho-RELA) in LTBR or tNGFR T cells stimulated with CD3/CD28 antibodies for the indicated periods of time. **h**, **i**, Quantification of phosphorylated IκBα (**h**) or mature NF-κB2 (**i**) in resting or CD3/CD28-stimulated (15 min) LTBR or tNGFR cells. **j**, IFNγ secretion by stimulated LTBR or tNGFR cells after CRISPR knockout of the indicated genes ($n = 18$, 3 sgRNAs in 2 donors in 3 biological replicates). IFNγ quantities are normalized to corresponding non-targeting (NT) controls (either LTBR or tNGFR) to allow comparisons of the relative effects of gene knockout on T cell activation. **k**, Expression levels of core LTBR genes ($n = 274$ genes) in LTBR and tNGFR cells after CRISPR knockout of *RELA* or *RELB* (normalized to non-targeting control in LTBR cells). Boxes show 25th–75th percentiles with a line at the median; whiskers extend to 1.5 times the interquartile range. Unpaired two-sided *t* test *P* values (**c**, **g**–**k**): not significant (NS) $P > 0.05$, $^*P < 0.05$, $^{**}P < 0.01$, $^{***}P < 0.001$, $^{****}P < 0.0001$ (exact *P* values are in Supplementary Table 15). Error bars, s.e.m.; $n = 3$ biological replicates, unless stated otherwise.

LTBR, whereas the deletion of residues 377–435 completely abrogated the LTBR phenotype, despite being expressed at a comparable—if not higher—level (Extended Data Fig. 6k), probably owing to the loss of a binding site for TRAF2, TRAF3 or TRAF5[29]. Moreover, a deletion of the self-association domain[30] (324–377) also completely abrogated the phenotype.

LTBR acts through canonical NF-κB in T cells

LTBR overexpression was shown to induce broad transcriptomic changes in T cells, accompanied by changes in T cell function (Fig. 4a, b). Thus, we sought to determine whether the perturbations in gene expression in LTBR cells were accompanied by epigenetic alterations, leveraging the assay for transposase-accessible chromatin by sequencing (ATAC-seq) (Extended Data Fig. 7a–g). Comparing the enrichments of specific transcription factor motifs in differentially accessible chromatin regions, we identified NF-κB p65 (RELA) as the most enriched transcription factor in LTBR cells (Extended Data Fig. 7h, i). Of note, NF-κB p65 and NFAT–AP-1 were the two most enriched transcription factors in open chromatin in stimulated versus resting T cells (both LTBR and tNGFR), in line with their well-established role in T cell activation[31], but only NF-κB p65 showed strong enrichment in LTBR cells, with and without stimulation (Fig. 4f). This result suggests that LTBR induces a partial T cell activation state but still requires signal 1 (TCR stimulation) for full activation.

We then decided to investigate changes in protein expression and/or phosphorylation of the members of the NF-κB signalling pathway. We observed a more rapid phosphorylation of p65 (RELA) and a strong increase in phosphorylation of an NF-κB inhibitor, IκBα, targeting IκBα for degradation; both of these effects enhance NF-κB activation or transcription (Fig. 4g, h, Extended Data Fig. 8a–c). In addition to changes in the canonical NF-κB pathway, we also detected an upregulation of key mediators of the non-canonical NF-κB pathway, RELB and NF-κB p52 (Fig. 4i, Extended Data Fig. 8b, c).

Having established that LTBR activates both the canonical and the non-canonical NF-κB pathways, we sought to determine the molecular basis of this phenomenon by perturbing key genes in the LTBR and NF-κB pathways by co-delivery of LTBR or tNGFR and CRISPR constructs that target 11 genes involved in the LTBR signalling pathway[32] (Fig. 4j, Extended Data Fig. 8d–o). Knockout of *LTB*, *TRAF2* and *NIK* (also known as *MAP3K14*) significantly reduced the secretion of IFNγ from LTBR cells but not (or to a lesser extent) from control (tNGFR) cells, whereas perturbations of *LIGHT* (also known as *TNFSF14*), *ASK1* (also known as *MAP3K5*) and *RELA* had a stronger effect on control cells than on LTBR cells. The effect of LTB loss on T cell activation in LTBR cells supports the observation that alanine mutagenesis of key residues involved in LTA or LTB binding (Fig. 4e) partially reduced the LTBR phenotype. Notably, we observed that loss of either TRAF2 or TRAF3 boosted IFNγ secretion in tNGFR cells only, in line with previous findings that T cells from TRAF2 dominant negative mice are hyperresponsive to TCR stimulation[33].

To investigate the potential roles of canonical versus non-canonical NF-κB signalling in LTBR T cells, we decided to analyse the global effects of RELA or RELB loss on the LTBR-driven gene expression profiles. Using bulk RNA-seq on T cells overexpressing LTBR or tNGFR, we discovered that only the loss of RELA significantly downregulated the expression of 'core' LTBR genes, whereas loss of RELB had no effect (Fig. 4k, Extended Data Fig. 8p).

ORFs enhance antigen-specific responses

Thus far we have shown that top-ranked genes from the ORF screen improve T cell function using a non-specific, pan-TCR stimulation. We next sought to determine whether a similar improvement could be observed using antigen-specific stimulation (Fig. 5a). To that end, we co-expressed several top-ranked genes with two FDA-approved CARs that target CD19, a B cell marker (Extended Data Fig. 9a–d). Using LTBR as an example, we demonstrated that ORF expression is achievable with this tricistronic vector (Extended Data Fig. 9e–i).

Since both CARs use different costimulatory domains, from CD28 or 4-1BB, we wanted to determine whether top-ranked genes that were selected using CD28 co-stimulation could also work in the context of 4-1BB co-stimulation. Nearly all of the top-ranked genes tested, with the exception of *AKR1C4*, improved upregulation of CD25 and antigen-specific cytokine secretion, with no major differences in the differentiation or exhaustion phenotype (Fig. 5b, c, Extended Data Figs. 9j–p, 10a–d).

Although production of IL-2 and IFNγ is crucial for the clonal expansion and antitumour activity of T cells, another vital component of tumour immunosurveillance is direct cytotoxicity. Top-ranked genes had an overall stronger effect on the cytotoxicity of CD28 CAR T cells than 4-1BB CAR T cells (Fig. 5d–f, Extended Data Fig. 10e, f). Notably, we observed that CAR T cells co-expressing LTBR tended to form large cell clusters; these clusters were typically absent in wells with control cells but are consistent with the overall higher expression of adhesion molecules such as ICAM-1 in LTBR-expressing cells (Extended Data Fig. 10g). Another important feature of effective antitumour T cells is the ability to maintain functionality despite chronic antigen exposure. In line with our previous findings in the context of LTBR alone (Fig. 4d), CAR T cells expressing LTBR showed a better functionality than matched CAR T cells expressing tNGFR after repeated challenge with target cells (Fig. 5g, Extended Data Fig. 10h–j).

T cells from healthy donors are relatively easy to engineer and rarely show signs of dysfunction in culture, whereas autologous T cells in patients with cancer are often dysfunctional, showing limited proliferation and effector functions[34]. To investigate whether top-ranked genes can improve CAR T cell response not only in healthy T cells but also in potentially dysfunctional T cells derived from patients, we transduced CD19 CARs co-expressed with LTBR or a control gene into peripheral blood mononuclear cells (PBMCs) from patients with diffuse large B cell lymphoma. After co-incubation with $CD19^+$ target cells, we observed a similar increase in the secretion of IL-2 and IFNγ from LTBR CAR T cells to that seen in healthy donors, indicating that identified ORFs can be successfully used to engineer T cells from patients with lymphoma ex vivo (Fig. 5h, Extended Data Fig. 10k). Of note, there was no secretion of cytokines in response to $CD19^-$ cells, indicating that overexpression of LTBR does not induce a spurious, antigen-independent response.

The screen and subsequent validations were performed in αβ T cells, the predominant subset of T cells in human peripheral blood. Although immunotherapy based on αβ T cells has shown considerable potential in the clinic, γδ T cells present an attractive alternative, owing to their lack of MHC restriction, ability to target broadly expressed stress markers in a cancer-type-agnostic manner and more innate-like characteristics[5]. We therefore sought to determine whether the top genes validated in αβ T cells translated to γδ T cells. After co-incubation with leukaemia or pancreatic ductal adenocarcinoma cancer cells, we observed an increase in IL-2 and IFNγ secretion from γδ T cells that were transduced with top-ranked genes (Fig. 5i, Extended Data Fig. 10l–p). Thus, top-ranked genes from our screen can act on signalling pathways that are conserved between even highly divergent T cell subsets, highlighting their broad applicability for cancer immunotherapy.

Discussion

In summary, here we developed a genome-scale gain-of-function screen in primary human T cells, in which we examined the effects of nearly 12,000 full-length genes on TCR-driven proliferation in a massively parallel manner. The largest—to our knowledge—previously published gain-of-function study in primary T cells involved 36 constructs, including full-length genes and synthetic receptors[35]. That approach relied on construct delivery via donor DNA and Cas9-mediated targeted insertion. Although using donor DNA for target gene delivery allows for more flexibility in terms of construct design, especially for engineering synthetic receptors, that method is less scalable and less accessible in terms of cost and complexity than the lentiviral library that we used here. Thus, we believe that ORF-based gain-of-function screens are readily applicable to a plethora of T cell phenotypes and settings, and that they offer the opportunity for clinical translation. In fact, all FDA-approved CAR therapies already rely on lentiviral or retroviral integration of a CAR transgene, and therefore an addition of an ORF to this system should pose no major manufacturing or regulatory challenges. The use of ORF-encoding mRNA delivered to CAR T cells before infusion is another translational route, especially if there are safety concerns about the mode of action of a particular ORF.

Gain-of-function screens have the potential to uncover regulators that are tightly controlled, restricted to a specific developmental stage or expressed only in certain circumstances. As shown here, LTBR is canonically absent from cells of lymphoid origin, but, owing to the intact signalling pathway, it can have a synthetic role when introduced to T cells. Although constitutive activation of other TNFRSF members might result in a similar phenotype, one of the features that distinguishes LTBR (and plausibly led to its enrichment, but not that of other TNFRSF members, in the screen) is the formation of an autocrine loop whereby the receptor and its ligands are present in the same cell. It is particularly noteworthy that expression of LTBR boosts IL-2 secretion, as this cytokine is produced exclusively by T cells and not by cell types that endogenously express LTBR. In addition to boosting cytokine secretion, overexpression of LTBR promoted stemness (expression of TCF1) and decreased activation-induced apoptosis, as well as offered a level of protection against phenotypic and functional hallmarks of T cell exhaustion—all of which are features not recapitulated by cell types that endogenously express LTBR. Previous work using overexpression of LTBR in cell lines showed that LTBR has a pro-apoptotic role[36], in direct contrast to the phenotype that we observed in primary T cells. Transcript- and protein-level analyses revealed that LTBR drives

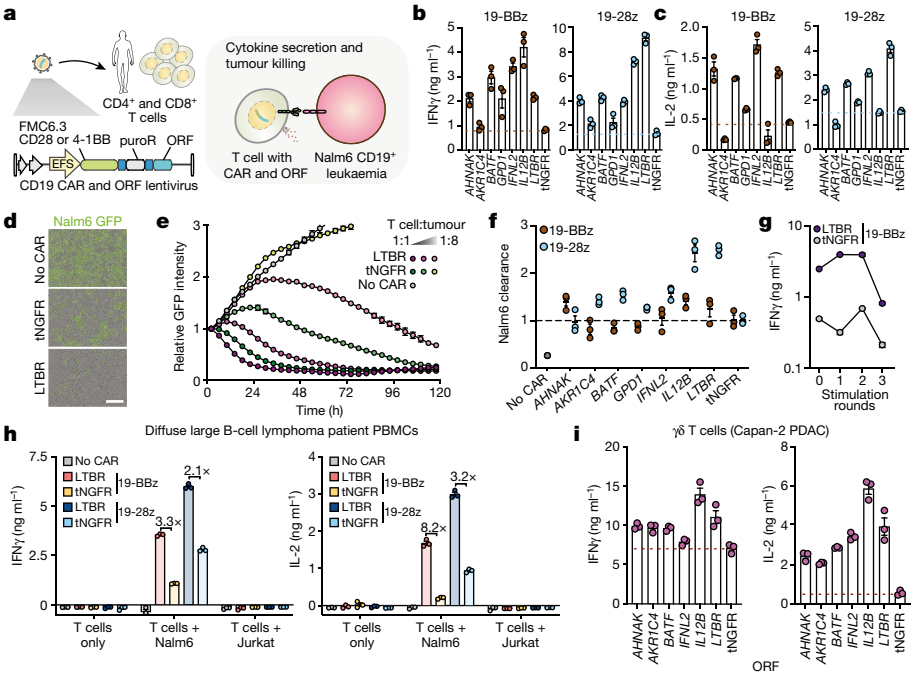

Fig. 5 | Top-ranked genes improve antigen-specific T cell responses and tumour killing. a–**g**, Co-delivery of anti-CD19 CARs and ORFs to T cells from healthy donors. **a**, Schematic of tricistronic vector and CAR T cell experiments. **b**, **c**, Secretion of IFNγ (**b**) and IL-2 (**c**) after overnight co-incubation of $CD8^+$ T cells with Nalm6 cells at a 1:1 ratio ($n = 3$ biological replicates, representative of 2 donors). **d**, Representative images of Nalm6 GFP^+ cells co-incubated for 48 h with CAR T cells or untransduced control T cells. Scale bar, 200 µm. **e**, Nalm6 GFP^+ cell proliferation (normalized total GFP per well) after co-incubation with T cells co-expressing 19-28z CAR and LTBR or tNGFR (negative control) at the indicated effector-to-target ratios. **f**, Quantification of Nalm6 GFP^+ clearance for T cells co-expressing 19-28z or 18-BBz CARs and top-ranked genes ($n = 3$ biological replicates, representative of 2 donors), normalized to tNGFR at an effector-to-target ratio of 0.25 and after 48 h of co-incubation. **g**, 19-BBz CAR T cells co-expressing LTBR or tNGFR were co-incubated at a 1:1 ratio with Nalm6 cells every 3 days for up to 3 rounds of stimulation ($n = 3$ biological replicates). Seven days after repeated antigen stimulation, CAR T cells were re-exposed to Nalm6 cells. IFNγ secretion was measured after overnight incubation. **h**, Co-delivery of anti-CD19 CARs and ORFs to total PBMCs from a patient with diffuse large B cell lymphoma. Transduced T cells were incubated alone, or co-incubated with $CD19^+$ Nalm6 or $CD19^-$ Jurkat cell lines at a 1:1 ratio ($n = 3$ biological replicates, representative of 2 patients). Secretion of IFNγ and IL2 was measured after overnight incubation. For the Nalm6 condition, numbers above indicated column pairs are the fold increase in cytokine secretion by LTBR cells over tNGFR (negative control) cells. **i**, Delivery of ORFs to Vγ9Vδ2 T cells. Secretion of IFNγ and IL-2 after overnight co-incubation with the pancreatic ductal adenocarcinoma (PDAC) line Capan-2, pre-treated with zoledronate to boost phosphoantigen accumulation ($n = 3$ biological replicates). Data are mean ± s.e.m. where appropriate.

the constitutive activation of both canonical and non-canonical NF-κB pathways. However, using epigenomic profiling and CRISPR-based functional perturbations we showed that the phenotypic and functional changes resulting from LTBR expression are mediated primarily through activation of the canonical NF-κB pathway, whereas changes in the non-canonical pathway may not be essential for the observed phenotypes—in contrast to the well-established role of non-canonical NF-κB activation in cells that endogenously express LTBR[37].

Gene overexpression has been used for pre-clinical enhancement of CAR T cell therapies in numerous studies. For example, armouring CAR T cells with cytokines such as IL-12 or IL-18, which are not typically produced by T cells but are known to improve T cell function when secreted by other cell types, was shown to improve their antitumour activity[38,39]. Notably, a previous study found that CAR T cell exhaustion can be alleviated by overexpression of c-JUN, a transcription factor identified by RNA-seq as specifically depleted in exhausted cells[40]. We suggest that enhancing CAR T cells through expression of LTBR (full-length or a truncated version) and other top-ranked genes identified here could result in the development of a new generation of cellular therapies. We envision further extensions of the screening approach presented here to more sophisticated models, for instance involving co-culture of edited T cells with antigen-presenting or immunosuppressive cells to identify genes that can modulate cell–cell cross-talk, a crucial feature of the immune response. Future studies that adapt genome-wide gain-of-function screens to relevant models of immunotherapy will lead to advanced target selection for engineering synthetic cellular therapies that can overcome the immunosuppressive tumour microenvironment and eradicate established cancers.

Online content

Any methods, additional references, Nature Research reporting summaries, source data, extended data, supplementary information, acknowledgements, peer review information; details of author contributions and competing interests; and statements of data and code availability are available at https://doi.org/10.1038/s41586-022-04494-7.

1. Abramson, J. S. et al. Transcend NHL 001: immunotherapy with the CD19-directed CAR T-cell product JCAR017 results in high complete response rates in relapsed or refractory B-cell non-Hodgkin lymphoma. *Blood* **128**, 4192–4192 (2016).
2. Shifrut, E. et al. Genome-wide CRISPR screens in primary human T cells reveal key regulators of immune function. *Cell* **175**, 1958–1971 (2018).
3. Dong, M. B. et al. Systematic immunotherapy target discovery using genome-scale in vivo CRISPR screens in CD8 T cells. *Cell* **178**, 1189–1204 (2019).
4. Chen, Z. et al. In vivo $CD8^+$ T cell CRISPR screening reveals control by Fli1 in infection and cancer. *Cell* **184**, 1262–1280 (2021).
5. Kabelitz, D., Serrano, R., Kouakanou, L., Peters, C. & Kalyan, S. Cancer immunotherapy with γδ T cells: many paths ahead of us. *Cell. Mol. Immunol.* **17**, 925–939 (2020).
6. Munshi, N. C. et al. Idecabtagene vicleucel in relapsed and refractory multiple myeloma. *N. Engl. J. Med.* **384**, 705–716 (2021).
7. Fraietta, J. A. et al. Determinants of response and resistance to CD19 chimeric antigen receptor (CAR) T cell therapy of chronic lymphocytic leukemia. *Nat. Med.* **24**, 563–571 (2018).

8. Singer, M. et al. A distinct gene module for dysfunction uncoupled from activation in tumor-infiltrating T cells. *Cell* **166**, 1500–1511 (2016).
9. Gurusamy, D. et al. Multi-phenotype CRISPR–Cas9 screen identifies p38 kinase as a target for adoptive immunotherapies. *Cancer Cell* **37**, 818–833 (2020).
10. Legut, M., Dolton, G., Mian, A. A., Ottmann, O. G. & Sewell, A. K. CRISPR-mediated TCR replacement generates superior anticancer transgenic T cells. *Blood* **131**, 311–322 (2018).
11. Ren, J. et al. Multiplex genome editing to generate universal CAR T cells resistant to PD1 inhibition. *Clin. Cancer Res.* **23**, 2255–2266 (2017).
12. Wagner, D. L. et al. High prevalence of *Streptococcus pyogenes* Cas9-reactive T cells within the adult human population. *Nat. Med.* **25**, 242–248 (2019).
13. Wu, X. et al. Genome-wide binding of the CRISPR endonuclease Cas9 in mammalian cells. *Nat. Biotechnol.* **32**, 670–676 (2014).
14. Sack, L. M. et al. Profound tissue specificity in proliferation control underlies cancer drivers and aneuploidy patterns. *Cell* **173**, 499–514 (2018).
15. Yuan, J. et al. CTLA-4 blockade enhances polyfunctional NY-ESO-1 specific T cell responses in metastatic melanoma patients with clinical benefit. *Proc. Natl Acad. Sci. USA* **105**, 20410–20415 (2008).
16. Sommermeyer, D. et al. Chimeric antigen receptor-modified T cells derived from defined $CD8^+$ and $CD4^+$ subsets confer superior antitumor reactivity in vivo. *Leukemia* **30**, 492–500 (2016).
17. Fischer, A. M., Katayama, C. D., Pagès, G., Pouysségur, J. & Hedrick, S. M. The role of Erk1 and Erk2 in multiple stages of T cell development. *Immunity* **23**, 431–443 (2005).
18. Lipp, A. M. et al. Lck mediates signal transmission from CD59 to the TCR/CD3 pathway in Jurkat T cells. *PLoS One* **9**, e85934 (2014).
19. Ma, X. et al. Interleukin-23 engineering improves CAR T cell function in solid tumors. *Nat. Biotechnol.* **38**, 448–459 (2020).
20. Seo, H. et al. BATF and IRF4 cooperate to counter exhaustion in tumor-infiltrating CAR T cells. *Nat. Immunol.* **22**, 983–995 (2021).
21. Jamali, A. et al. Highly efficient and selective CAR-gene transfer using CD4- and CD8-targeted lentiviral vectors. *Mol. Ther. Methods Clin. Dev.* **13**, 371–379 (2019).
22. Stoeckius, M. et al. Simultaneous epitope and transcriptome measurement in single cells. *Nat. Methods* **14**, 865–868 (2017).
23. Mimitou, E. P. et al. Multiplexed detection of proteins, transcriptomes, clonotypes and CRISPR perturbations in single cells. *Nat. Methods* **16**, 409–412 (2019).
24. Gil-Yarom, N. et al. CD74 is a novel transcription regulator. *Proc. Natl Acad. Sci. USA* **114**, 562–567 (2017).
25. Ataide, M. A. et al. BATF3 programs $CD8^+$ T cell memory. *Nat. Immunol.* **21**, 1397–1407 (2020).
26. Katagiri, T., Kameda, H., Nakano, H. & Yamazaki, S. Regulation of T cell differentiation by the AP-1 transcription factor JunB. *Immunol. Med.* **44**, 197–203 (2021).
27. Zhao, X., Shan, Q. & Xue, H.-H. TCF1 in T cell immunity: a broadened frontier. *Nat. Rev. Immunol*. https://doi.org/10.1038/s41577-021-00563-6 (2021).
28. Sudhamsu, J. et al. Dimerization of LTβR by LTα1β2 is necessary and sufficient for signal transduction. *Proc. Natl Acad. Sci USA* **110**, 19896–19901 (2013).
29. Li, C. et al. Structurally distinct recognition motifs in lymphotoxin-β receptor and CD40 for tumor necrosis factor receptor-associated factor (TRAF)-mediated signaling. *J. Biol. Chem.* **278**, 50523–50529 (2003).
30. Wu, M.-Y., Wang, P.-Y., Han, S.-H. & Hsieh, S.-L. The cytoplasmic domain of the lymphotoxin-β receptor mediates cell death in HeLa cells. *J. Biol. Chem.* **274**, 11868–11873 (1999).
31. Macian, F. NFAT proteins: key regulators of T-cell development and function. *Nat. Rev. Immunol.* **5**, 472–484 (2005).
32. Dejardin, E. et al. The lymphotoxin-β receptor induces different patterns of gene expression via two NF-κB pathways. *Immunity* **17**, 525–535 (2002).
33. Saoulli, K. et al. CD28-independent, TRAF2-dependent costimulation of resting T cells by 4-1BB ligand. *J. Exp. Med.* **187**, 1849–1862 (1998).
34. Thommen, D. S. & Schumacher, T. N. T cell dysfunction in cancer. *Cancer Cell* **33**, 547–562 (2018).
35. Roth, T. L. et al. Pooled knockin targeting for genome engineering of cellular immunotherapies. *Cell* **181**, 728–744 (2020).
36. VanArsdale, T. L. et al. Lymphotoxin- receptor signaling complex: role of tumor necrosis factor receptor-associated factor 3 recruitment in cell death and activation of nuclear factor B. *Proc. Natl Acad. Sci. USA* **94**, 2460–2465 (1997).
37. Yılmaz, Z. B. et al. Quantitative dissection and modeling of the NF-κB p100-p105 module reveals interdependent precursor proteolysis. *Cell Rep.* **9**, 1756–1769 (2014).
38. Hu, B. et al. Augmentation of antitumor immunity by human and mouse CAR T cells secreting IL-18. *Cell Rep.* **20**, 3025–3033 (2017).
39. Yeku, O. O., Purdon, T. J., Koneru, M., Spriggs, D. & Brentjens, R. J. Armored CAR T cells enhance antitumor efficacy and overcome the tumor microenvironment. *Sci. Rep.* **7**, 10541 (2017).
40. Lynn, R. C. et al. c-Jun overexpression in CAR T cells induces exhaustion resistance. *Nature* **576**, 293–300 (2019).
41. Schmiedel, B. J. et al. Impact of genetic polymorphisms on human immune cell gene expression. *Cell* **175**, 1701–1715 (2018).

Methods

Isolation and culture of primary human T cells

Regular buffy coats containing peripheral blood from de-identified healthy donors were collected by and purchased from the New York Blood Center under an IRB-exempt protocol. All donors provided informed consent. Peripheral blood mononuclear cells (PBMC) were isolated from buffy coats using Lymphoprep (Stemcell) gradient centrifugation. For most assays, $CD8^+$ and $CD4^+$ were isolated sequentially from the same donor. First, $CD8^+$ T cells were isolated by magnetic positive selection using the EasySep Human CD8 Positive Selection Kit II (Stemcell). Then, $CD4^+$ T cells were isolated from the resulting flowthrough by negative magnetic selection using the EasySep Human CD4+ T cell Isolation Kit (Stemcell). γδ T cells were isolated by magnetic negative selection using the EasySep Human Gamma/Delta T cell Isolation Kit (Stemcell). Immediately after isolation, T cells were resuspended in T cell medium, which consisted of Immunocult-XF T cell Expansion Medium (Stemcell) supplemented with 10 ng ml^{-1} recombinant human IL-2 (Stemcell).

Activation of T cells was performed with Immunocult Human CD3/CD28 T cell Activator (Stemcell) using 25 µl per 10^6 cells per ml. Typically, T cells were transduced with concentrated lentivirus 24 h after isolation. For some experiments, T cells were electroporated with in-vitro-transcribed mRNA 24 h after isolation or with Cas9 protein 48 h after isolation. At 72 h after isolation, lentivirally transduced T cells were selected with 2 µg ml^{-1} puromycin.

Every 2–3 days, T cells were either split or had the medium replaced to maintain a cell density of 1×10^6–2×10^6 cells per ml. Lentivirally transduced T cells were maintained in medium containing 2 µg ml^{-1} puromycin for the duration of culture. T cells were used for phenotypic or functional assays between 14 and 21 days after isolation, or cryopreserved in Bambanker Cell Freezing Medium (Bulldog Bio). γδ T cells were further purified before functional assays using anti-Vγ9 PE antibody (Biolegend) and anti-PE microbeads (Miltenyi Biotec) according to the manufacturer's recommendations, in the presence of dasatinib, a protein kinase inhibitor, to prevent activation-induced cell death resulting from TCR cross-linking[42]. PBMCs from patients with diffuse large B cell lymphoma were obtained from the Perlmutter Cancer Center under a protocol approved by the Perlmutter Cancer Center Institutional Review Board (S14-02164).

Vector design and molecular cloning

All vectors used were cloned using Gibson Assembly (NEB). For the experiments shown in Fig. 1, we used the lentiviral backbone from the pHAGE plasmid[14]. For all other experiments, the backbone from lentiCRISPRv2 (Addgene 52961) was used. ORFs were PCR-amplified for cloning from the genome-scale library used in the screen.

After adding Gibson overhangs by PCR, ORFs and P2A-puro were inserted into XbaI- and EcoRI-cut lentiCRISPRv2. The sgRNA cassette was removed from lentiCRISPRv2 using PacI and NheI digest. For *LTBR* overexpression and knockout experiments, the sgRNA cassette was not removed. CARs were synthesized as gBlocks (IDT). For CAR-ORF cloning, CAR-P2A-puro-T2A(partial) were first inserted into XbaI- and EcoRI-cut lentiCRISPRv2. For subsequent ORF insertion, the plasmid was cut with HpaI located within the partial T2A and EcoRI. The following vectors were deposited to Addgene: pOT_01 (lenti-EFS-LTBR-2A-puro, Addgene 181970), pOT_02 (lenti-EFS-tNGFR-2A-puro, Addgene 181971), pOT_03 (lenti-EFS-FMC6.3-28z-2A-puro-2A-LTBR, Addgene 181972), pOT_04 (lenti-EFS-FMC6.3-BBz-2A-puro-2A-LTBR, Addgene 181973), pOT_05 (lenti-EFS-FMC6.3-28z-2A-puro-2A-tNGFR, Addgene 181974) and pOT_06 (lenti-EFS-FMC6.3-BBz-2A-puro-2A-tNGFR, Addgene 181975).

Nuclease and CRISPR guide RNA design

All sgRNAs were designed using the GUIDES webtool[43]. We selected guides that target initial protein-coding exons (with the preference for targeting protein family domains enabled in GUIDES) as well as minimizing off-target and maximizing on-target scores (Supplementary Table 16). For Cas9 nuclease nucleofection, we used purified sNLS-SpCas9-sNLS nuclease (Aldevron).

Preparation of ORF library plasmids for paired-end sequencing

We re-amplified a previously described genome-scale ORF library[14] using Endura electrocompetent cells (Lucigen). The identity of ORFs and matched barcodes was confirmed by paired-end sequencing (Supplementary Table 1). In brief, the plasmid was first linearized with I-SceI meganuclease, which cuts downstream of the barcode. Then, the linearized plasmid was tagmented using TnY transposase[44]. Then, the fragmented plasmid was amplified in a PCR reaction, using a forward primer binding to a handle introduced by TnY and a reverse primer binding to a sequence downstream of the barcode. All transposons and PCR primer oligonucleotides were synthesized by IDT (Supplementary Table 2). The resulting amplicon was sequenced on a NextSeq 500. The forward read (containing the ORF) was mapped to GRCh38.101 CDS transcriptome annotations using STAR v.2.7.3a (map quality ≥ 10)[45]. Using the paired-end read, we also captured the 24 nucleotide barcode downstream of the constant plasmid sequence. We tabulated ORF–barcode combinations and further curated this table by eliminating any spurious pairs that might be due to sequencing or PCR error. Specifically, a permutation test was performed to identify the maximum number of ORF–barcode combinations expected by random chance, after which we only kept ORF–barcode combinations with a count that exceeded this maximum number. We excluded all non-coding elements from the reference and then collapsed barcodes that were within a Levenshtein distance less than 2.

Cell culture

HEK293FT cells were obtained from Thermo Fisher Scientific and cultured in Dulbecco's modified Eagle's medium (DMEM) supplemented with 10% Serum Plus-II (Thermo Fisher Scientific). Nalm6, Jurkat and BxPC3 cells were obtained from ATCC and cultured in RPMI-1640 supplemented with 10% Serum Plus-II. Capan-2 cells were obtained from ATCC and cultured in McCoy's medium supplemented with 10% Serum Plus-II. For γδ co-incubation experiments, cell lines were pre-treated with 50 µM zoledronic acid (Sigma) for 24 h. Cell lines were routinely tested for mycoplasma using MycoAlert PLUS (Lonza) and found to be negative. Cell lines were not authenticated in this study.

Lentivirus production

We produced lentivirus by co-transfecting third-generation lentiviral transfer plasmids together with packaging plasmid psPAX2 (Addgene 12260) and envelope plasmid pMD2.G (Addgene 12259) into HEK293FT cells, using polyethyleneimine linear MW 25000 (Polysciences). After 72 h, we collected the supernatants, filtered them through a 0.45-µm Steriflip-HV filter (Millipore) and concentrated the virus using Lentivirus Precipitation Solution (Alstem). Concentrated lentivirus was resuspended in T cell medium containing IL-2 and stored at −80 C°.

Pooled ORF library screening

For pooled ORF library screening, $CD4^+$ and $CD8^+$ T cells were isolated from a minimum of 500×10^6 PBMCs from 3 healthy donors. The amount of lentivirus used for transduction was titrated to result in 20–30% transduction efficiency, to minimize the probability of multiple ORFs being introduced into a single cell. The cells were maintained in T cell medium containing 2 µg ml^{-1} puromycin and counted every 2–3 days to maintain a cell density of 1×10^6–2×10^6 cells per ml. On day 14 after isolation, T cells were collected, counted, labelled with 5 µM CFSE (Biolegend) and stimulated with CD3/CD28 Activator (Stemcell) at 1.56 µl per 1×10^6 cells. An aliquot of cells representing 1,000× coverage of the library was frozen down at this step to be used as a pre-stimulation control. After 4 days of stimulation, cells were collected and an aliquot of cells representing 1,000× coverage of the library was frozen down to be used as a pre-sort control. The remaining cells were stained with

LIVE/DEAD Violet cell viability dye (Thermo Fisher Scientific), and CFSE^{low} cells (corresponding to the bottom 15% of the distribution) were sorted using a Sony SH800S cell sorter (all antibodies and dyes are listed in Supplementary Table 3). Genomic DNA was isolated, and two rounds of PCR to amplify ORF barcodes and add Illumina adaptors were performed[46] (Supplementary Table 2).

Pooled ORF screen analysis

For most of the analyses, equal numbers of reads from all three donors were combined per bin before trimming and alignment. The barcodes were mapped to the reference library after adaptor trimming with Cutadapt v.1.13 (-m 24 -e 0.1 --discard-untrimmed) using Bowtie v.1.1.2 (-v 1 -m 1 --best --strata)[47,48]. All subsequent analyses were performed in RStudio v.1.1.419 with R 4.0.0.2. To calculate individual barcode enrichment, barcode counts were normalized to the total number of reads per sample (with pseudocount added) and $\log_2$-transformed. To calculate ORF enrichment, raw barcode counts were first collapsed by genes before normalization and $\log_2$ transformation.

We performed enrichment analyses at both the barcode and gene level (Supplementary Tables 4, 5). Statistical analysis on barcode enrichment was performed using MAGeCK[49], comparing CFSE^{low} samples to corresponding inputs (pre-stimulation), using CD4$^+$ and CD8$^+$ as replicates. Statistical analysis on ORF enrichment was performed using DESeq2[50]. We obtained raw gene counts by collapsing barcodes into corresponding genes. CFSE^{low} samples were compared to corresponding inputs (both pre-stimulation and pre-sort), using CD4$^+$ and CD8$^+$ as replicates. GO enrichment (biological process) on genes passing DESeq2 criteria ($\log_2$-transformed fold change > 0.5, $P_{adj} < 0.05$) was performed using the topGO package[51]. For the genes enriched in the CFSE^{low} screen (DESeq2 analysis), we overlapped these genes with differentially expressed genes after CD3/CD28 stimulation using data from the Database of Immune Cell eQTLs, Expression, Epigenomics (DICE; https://dice-database.org/)[41]. For differentially expressed genes, we used the following DICE datasets: 'T cell, CD4, naive' versus 'T cell, CD4, naive [activated]', 'T cell, CD8, naive' versus 'T cell, CD8, naive [activated]'. Significant differential expression was as given in the DICE dataset ($P_{adj} < 0.05$).

Proliferation assays

Transduced T cells were collected at day 14 after isolation, counted and plated at 2.5×10^4 cells per well in a round bottom 96-well plate, in 2 sets of triplicate wells per transduction. One set of triplicate wells was cultured in Immunocult-XF T cell Expansion Medium supplemented with 10 ng ml^{-1} IL-2 and another set of triplicate wells was further supplemented with 1.56 µl CD3/CD28 Activator per 1 ml of medium. The cells were cultured for 4 days, and then were collected and stained with LIVE/DEAD Violet cell viability dye. Before flow cytometric acquisition, the cells were resuspended in D-PBS with 10% v/v Precision Counting Beads (Biolegend). For quantification, the number of viable cell events was normalized to the number of bead events per sample. Then, for each ORF the normalized number of viable cells in wells supplemented with CD3/CD28 Activator was divided by the mean number of viable cells in control wells to quantify T cell proliferation. To enable comparisons between donors and CD4$^+$/CD8$^+$ T cells, the proliferation of T cells transduced with a given ORF was finally normalized to the proliferation of a matched tNGFR control.

In addition to the counting beads assay, we also measured proliferation using a dye dilution assay. For this assay, transduced T cells were collected at day 14 after isolation, washed with D-PBS and then labelled with 5 µM CellTrace Yellow (CTY) in D-PBS for 20 min at room temperature. The excess dye was removed by washing with a fivefold excess of RPMI-1640 supplemented with 10% Serum Plus-II. The labelled cells were then plated at 2.5×10^4 cells per well on a round bottom 96-well plate. One set of triplicate wells was cultured in unsupplemented Immunocult-XF T cell Expansion Medium (that is, without IL-2) and another set of triplicate wells was supplemented with 10 ng ml^{-1} IL-2 and 1.56 µl CD3/CD28 Activator per 1 ml of medium. The cells were cultured for 4 days, and then were collected and stained with LIVE/DEAD Violet cell viability dye. For quantification of the proliferation index, events were first gated on viable T cells in FlowJo (Treestar) and exported for further analysis in R/RStudio using the flowFit and flowCore packages[52]. Unstimulated cells were used to determine the parent population size and position to account for differences in staining intensity between different samples. These fitted parent population parameters were then used to fit the CTY profiles of matched stimulated samples, modelled as Gaussian distributions assuming $\log_2$-distanced peaks as a result of cell division and dye dilution. Fitted CTY profiles were inspected visually for concordance with the original CTY profiles and used to calculate the proliferation index. The proliferation index is defined as the sum of cells in all generations divided by the computed number of parent cells present at the beginning of the assay.

Flow cytometry for cell-surface and intracellular markers

All antibodies and dyes used for flow cytometry are listed in Supplementary Table 3. For CD25 (IL2RA) and CD154 (CD40L) quantification, T cells were restimulated with CD3/CD28 Activator (6.25 µl per 10^6 cells) for 6 h (CD154 staining in CD8$^+$) or for 24 h before staining (CD25 staining in both CD4$^+$ and CD8$^+$, and CD154 staining in CD4$^+$). For Ki-67 and 7-amino-actinomycin D (7-AAD) staining, T cells were rested overnight in Immunocult-XF T cell Expansion Medium without IL-2 and then activated with CD3/CD28 Activator (25 µl per 10^6 cells) for 24 h. In other cases, T cells were stained without stimulation. For detection of secreted proteins, T cells were stimulated for 24 h with CD3/CD28 Activator (25 µl per 10^6 cells) (LTA, LIGHT), and protein transport inhibitors brefeldin A (5 µg ml^{-1}) and monensin (2 µM) were included for the last 6 h of stimulation (IL12B, LTA, LIGHT).

First, the cells were collected, washed with D-PBS and stained with LIVE/DEAD Violet cell viability dye for 5 min at room temperature in the dark, followed by surface antibody staining for 20 min on ice. After surface antibody staining (where applicable) the cells were washed with PBS and acquired on a Sony SH800S cell sorter or taken for intracellular staining. For intracellular staining, the cells were resuspended in an appropriate fixation buffer. The following fixation buffers were used for specific protein detection: Fixation Buffer (Biolegend) for IL12B and MS4A3 staining; True-Nuclear Transcription Factor Fix (Biolegend) for BATF, TCF1 and FLAG staining; and FoxP3/Transcription Factor Fixation Reagent, (eBioscience) for Ki-67. After resuspension in the fixation buffer, cells were incubated at room temperature in the dark for 1 h. Following the incubation, the cells were washed twice in the appropriate permeabilization buffer. The following permeabilization buffers were used: Intracellular Staining Permeabilization Wash Buffer (Biolegend) for IL12B and MS4A3 staining; True-Nuclear Perm Buffer (Biolegend) for BATF, TCF1 and FLAG staining; and FoxP3/Transcription Factor Permeabilization Buffer (eBioscience) for Ki-67. After permeabilization, the cells were stained with the specific antibody or isotype control for 30 min in the dark at room temperature. Finally, the cells were washed twice in the appropriate permeabilization buffer and acquired on a Sony SH800S flow cytometer. For cell-cycle analysis, the cells were further stained with 0.5 µg ml^{-1} 7-AAD for 5 min immediately before acquisition. Gating was performed using appropriate isotype, fluorescence minus one and biological controls. Typically, 5,000–10,000 live events were recorded per sample.

Flow cytometry detection of phosphorylated proteins

T cells were rested for 24 h in in Immunocult-XF T cell Expansion Medium without IL-2 before detection of phosphorylated proteins. The rested cells were stimulated with CD3/CD28 Activator (25 µl per 10^6 cells) for the times indicated in the corresponding figure. Immediately after the stimulation period, the cells were fixed with a 1:1 volume ratio of the pre-warmed Fixation Buffer (Biolegend) for 15 min at 37 °C and washed twice with the cell staining buffer (D-PBS + 2% FBS). As per the manufacturer's protocol, the cells were resuspended in the residual volume and permeabilized in 1 ml of pre-chilled True-Phos Perm Buffer (Biolegend)

while vortexing. The cells were incubated in the True-Phos Perm Buffer for 60 min at −20 °C. After permeabilization the cells were washed twice with the cell staining buffer and stained with anti-CD4, anti-CD8, anti-RELA and anti-phospho-RELA antibodies (or isotype controls) for 30 min at room temperature. After staining, the cells were washed twice in the cell staining buffer and acquired on a Sony SH800S cell sorter. Gating was performed on $CD4^+$ or $CD8^+$ cells, and the levels of RELA and phospho-RELA were determined using appropriate isotype and biological controls.

Western blot detection of proteins and phosphorylated proteins

T cells expressing tNGFR or LTBR, resting or stimulated for 15 min with CD3/CD28 Activator (25 µl per 10^6 cells), were collected, washed with 1× D-PBS and lysed with TNE buffer (10 mM Tris-HCl, pH 7.4, 150 mM NaCl, 1 mM EDTA, 1% Nonidet P-40) in the presence of a protease inhibitor cocktail (Bimake B14001) and a phosphatase inhibitor cocktail (Cell Signaling Technologies 5872S) for 1 h on ice. Cell lysates were spun for 10 min at 10,000*g*, and the protein concentration was determined with the BCA assay (Thermo Fisher Scientific). Equal amounts of cell lysates (25 mg) were denatured in Tris-Glycine SDS Sample buffer (Thermo Fisher Scientific) and loaded on a Novex 4–12 or 4–20 % Tris-Glycine gel (Thermo Fisher Scientific). The PageRuler pre-stained protein ladder (Thermo Fisher Scientific) was used to determine the protein size. The gel was run in 1× Tris-Glycine-SDS buffer (IBI Scientific) for about 120 min at 120 V. Proteins were transferred on a nitrocellulose membrane (BioRad) in the presence of prechilled 1× Tris-Glycine transfer buffer (Thermo Fisher Scientific) supplemented with 20% methanol for 100 min at 100 V.

Immunoblots were blocked with 5% skimmed milk dissolved in 1× PBS with 1% Tween-20 (PBST) and incubated overnight at 4 °C separately with the following primary antibodies: rabbit anti-GAPDH (0.1 mg ml^{-1}, Cell Signaling, 2118S), mouse anti-IKKα (1:1,000 dilution, Cell Signaling, 3G12), rabbit anti-IKKβ (1:1,000 dilution, Cell Signaling, D30C6), rabbit anti-NF-κB p65 (1:1,000 dilution, Cell Signaling, D14E12), rabbit anti-phospho-NF-κB p65 Ser536 (1:1,000 dilution, Cell Signaling, 93H1), mouse anti-IκBα (1:1,000 dilution, Cell Signaling, L35A5), rabbit anti-phospho-IκBα Ser32 (1:1,000 dilution, Cell Signaling, 14D4), rabbit anti-NF-κB p100/p52 (1:1,000 dilution, Cell Signaling, 4882) and rabbit anti-RELB (1:1,000 dilution, Cell Signaling, C1E4). After the primary antibody, the blots were incubated with IRDye 680RD donkey anti-rabbit (0.2 mg ml^{-1}, LI-COR 926–68073) or with IRDye 800CW donkey anti-mouse (0.2 mg ml^{-1}, LI-COR 926–32212). The blots were imaged using Odyssey CLx (LI-COR) and quantified using ImageJ v.1.52. The uncropped and unprocessed blots are shown in Supplementary Fig. 1.

Quantification of cytokine secretion

For measurement of secreted IFNγ and IL-2, T cells were first collected and rested for 24 h in medium without IL-2. Then, they were counted, plated at 2.5×10^4 cells per well in a round bottom 96-well plate and incubated in medium without IL-2, with or without CD3/CD28 Activator (25 µl per 10^6 cells) for 24 h. Then, cell supernatants were collected, diluted and used for cytokine quantification with an enzyme-linked immunosorbent assay (Human IL-2 or IFNγ DuoSet, R&D Systems), using an Infinite F200 Pro (Tecan) plate reader. Multiplexed quantification of secreted cytokines and chemokines in resting or stimulated T cells (Supplementary Table 7) was performed using the Human Cytokine/Chemokine 48-Plex Discovery Assay Array (Eve Technologies).

T cell killing assays

$CD19^+$ Nalm6 cells were first transduced with a lentiviral vector encoding EGFPd2PEST-NLS and a puromycin resistance gene[53]. The transduced cells were kept in puromycin selection throughout the culture, to maintain stable EGFP expression, and puromycin was only removed from the medium before the killing assay. T cells were transduced with a vector encoding a CAR specific for CD19, using either a CD28 stalk, CD28 transmembrane and CD28 signalling domain or CD8 stalk and CD8 transmembrane domain with 4-1BB signalling domain, and CD3ζ signalling domain[54]. Fourteen days after transduction, transduced T cells were combined with 5×10^4 Nalm6 GFP^+ cells in triplicate at indicated effector:target ratios in a flat 96-well plate pre-coated with 0.01% poly-L-ornithine (EMD Millipore) in Immunocult medium without IL-2. The wells were then imaged using an Incucyte SX1, using 20× magnification and acquiring 4 images per well every 2 h for up to 120 h. For each well, the integrated GFP intensity was normalized to the 2 h time point, to allow the cells to fully settle after plating.

In vitro mRNA preparation

The template for in vitro transcription was generated by PCR from a plasmid encoding LTBR or tNGFR with the resulting amplicon including a T7 promoter upstream of the ORF (Supplementary Table 2). The purified template was then used for in vitro transcription with capping and poly-A tailing using the HiScribe T7 ARCA mRNA Kit with Capping (NEB).

Primary T cell nucleofection

Activated T cells were nucleofected with in-vitro-transcribed mRNA at 24 h after activation or with Cas9 protein at 48 h after activation. The cells were collected, washed twice in PBS and resuspended in P3 Primary Cell Nucleofector Solution (Lonza) at 5×10^5 cells per 20 µl. Immediately after resuspension, 1 µg mRNA or 10 µg Cas9 (Aldevron) were added (not exceeding 10% v/v of the reaction) and the cells were nucleofected using the E0−115 program on a 4D-Nucleofector (Lonza). After nucleofection the cells were resuspended in pre-warmed Immunocult medium with IL-2 and recovered at 37 °C with 5% CO_2 for 20 min. After recovery, the cells were plated at 1×10^6 cells per ml and used in downstream assays.

OverCITE-seq sample preparation and sequencing

For single-cell sequencing, $CD8^+$ T cells were individually transduced with ORFs and kept, separately, under puromycin selection for 14 days. Then, transduced cells were combined and split into two conditions: one was cultured for 24 h only in the presence of IL-2; the other was further supplemented with 6.25 µl CD3/CD28 Activator per 10^6 cells. After stimulation, the cells were collected, counted and resuspended in staining buffer (2% BSA + 0.01% Tween-20 in PBS) at 2×10^7 cells per ml. Then, 10% (v/v) Human TruStain FcX Fc Receptor Blocking Solution (Biolegend) was added, and the cells were incubated at 4 °C for 10 min. After Fc receptor blocking, the cell concentration was adjusted to 5×10^6 cells per ml and the stimulated and unstimulated cells were split into 4 conditions each. Each condition received a different oligonucleotide-conjugated (barcoded) cell hashing antibody to allow for pooling of different conditions in the same 10x Genomics Chromium lane[23]. After 20 min co-incubation on ice, the cells were washed 3 times with staining buffer and counted using Trypan blue exclusion. Cell viability was typically around 95%.

Then, cells stained with different hashing antibodies were pooled together at equal numbers and stained with the following oligonucleotide-conjugated (barcoded) antibodies for quantification of cell surface antigens: CD11c (0.1 µg), CD14 (0.2 µg), CD16 (0.1 µg), CD19 (0.1 µg), CD56 (0.2 µg), CD3 (0.2 µg), CD45 (0.01 µg), CD45RA (0.2 µg), CD45RO (0.2 µg), CD4 (0.1 µg), CD8 (0.1 µg), CD25 (0.25 µg), CD69 (0.25 µg) and NGFR (0.25 µg) (TotalSeq-C, Biolegend). The cells were stained for 30 min on ice, washed 3 times with staining buffer, resuspended in PBS and filtered through a 40-µm cell strainer. The cells were then counted and the concentration was adjusted to 1×10^6 ml^{-1}. For loading into the 10x Genomics Chromium, 3×10^4 cells were combined with Chromium Next GEM Single Cell 5′ v2 Master Mix (10x Genomics) supplemented with a custom reverse primer binding to the puromycin resistance cassette for boosting ORF transcript capture at the reverse transcription stage (Supplementary Table 2). The custom reverse primer was added at a 1:3 ratio to the poly-dT primer included in the Master Mix.

For cDNA amplification, additive primers for amplification of sample hashing and surface antigen barcodes were included[23], as well as a nested reverse primer binding to the puromycin resistance cassette

downstream of the ORF. Following cDNA amplification, SPRI beads were used for size selection of resulting PCR products: small-size (fewer than 300 bp) sample hashing and surface antigen barcodes were physically separated from larger cDNA and ORF amplicons for downstream processing. Sample hashing and surface antigen barcodes were also processed[22]. Amplified cDNA was then separated into three conditions, for construction of the gene expression library, αβ TCR library and ORF library. The ORF library was processed similarly to the αβ TCR library, using nested reverse primers binding downstream of the ORF (Supplementary Table 2). The quality of produced libraries was verified on BioAnalyzer using the High Sensitivity DNA kit (Agilent). The libraries were sequenced on a NextSeq 500. For the gene expression library, more than 25,000 reads per cell were generated. For other libraries, more than 5,000 reads per cell were generated.

OverCITE-seq data analysis

Gene expression unique molecular identifier (UMI) count matrices and TCR clonotypes were derived using 10x Genomics Cell Ranger 3.1.0. Hashtag oligo (HTO) and antibody UMI count matrices were generated using kallisto v.0.46.0[55] and bustools v.0.39.3[56]. ORF reads were first aligned to plasmid references using Bowtie2 v.2.2.8[57] and indexed to the associated ORF, after which kallisto and bustools were used to generate UMI count matrices. All modalities were normalized using a centred log ratio (CLR) transformation. Cell doublets and negatives were identified using the HTODemux[58] function and then excluded from downstream analysis. The UMI cut-off quantile for HTODemux was optimized to maximize singlet recovery using grid search with values between 0 and 1. ORF singlets were identified using MULTIseqDemux[59]. We then excluded cells with low-quality gene expression metrics and removed cells with fewer than 200 unique RNA features or greater than 5% of reads mapping to the mitochondrial transcriptome.

Count matrices were then loaded into and analysed with Seurat v.4.0.1[60]. Cell cycle correction and scaling of gene expression data was performed using the CellCycleScoring function with default genes, followed by scaling the data using the ScaleData function. Principal component (PC) optimization of the scaled and corrected data was then performed using JackStraw[61], in which we selected all PCs up to the first non-significant PC to use in clustering. Clustering of cells was performed using a shared nearest neighbour (SNN)-based clustering algorithm and visualized using UMAP dimensional reduction[62] to project cluster PCs into 2D space. Cluster marker analysis was performed using the FindAllMarkers function with the hypothesis set defined as positive and negative markers present in at least 25% of cluster cells and with a $\log_2$-transformed fold change threshold of 0.25 as compared to non-cluster cells (top genes per cluster are listed in Supplementary Table 8). Differential expression analysis of ORFs was performed using DESeq2[50] to identify genes up and downregulated in ORF-expressing cells as compared to NGFR (control) cells, with differential expression defined as those with $q < 0.1$ calculated using the Storey method[63].

Bulk RNA-seq and analysis

$CD4^+$ and $CD8^+$ LTBR- or tNGFR-transduced T cells were stimulated for 24 h with CD3/CD28 Activator (25 µl per 10^6 cells) or left unstimulated ($n = 3$ biological replicates). Total RNA was extracted using the Direct-zol RNA purification kit (Zymo). The 3′-enriched RNA-seq library was prepared as described before[64]. In brief, RNA was reverse-transcribed using SMARTScribe Reverse Transcriptase (Takara Bio) and a poly(dT) oligo containing a partial Nextera handle. The resulting cDNA was then PCR-amplified for 3 cycles using OneTaq polymerase (NEB) and tagmented for 5 min at 55 °C using homemade transposase TnY[44]. Immediately afterwards, the tagmented DNA was purified on a MinElute column (Qiagen) and PCR-amplified using OneTaq polymerase and barcoded primers for 12 cycles. The PCR product was purified using a dual (0.5×–0.8×) SPRI clean-up (Agencourt) and the size distribution was determined using Tapestation (Agilent). Samples were sequenced on a NextSeq 500 (Illumina) using a v2.5 75-cycle kit (paired end). Paired-end reads were aligned to the transcriptome (human Ensembl v.96 reference[65]) using kallisto v.0.46.0[55] and loaded into RStudio 1.1.419 with R 4.0.0.2 using the tximport package[66]. Differential gene expression analysis was performed using DESeq2[50] (Supplementary Tables 9–12). GO enrichment (biological process) on genes passing DESeq2 criteria ($\log_2$-transformed fold change > 1, $P_{adj} < 0.05$) was performed using the topGO package[51].

ATAC-seq library preparation

$CD8^+$ LTBR and tNGFR T cells were stimulated for 24 h with CD3/CD28 Activator (25 µl per 10^6 cells) or left unstimulated ($n = 2$ biological replicates). We performed bulk ATAC-seq as previously described[44]. In brief, cell membranes were lysed in the RSB buffer (10mM Tris-HCL pH 7.4, 3 mM $MgCl_2$, 10 mM NaCl) with 0.1% IGEPAL freshly added. After pipetting up and down, nuclei were isolated by centrifugation at 500*g* for 5 min at 4 °C. After discarding the supernatant, the nuclei were resuspended in the Tagmentation DNA (TD) Buffer[44] with homemade transposase TnY protein[44] and incubated at 37 °C for 30 min. After purification on a MinElute column (Qiagen), the tagmented DNA was PCR-amplified using a homemade Pfu X7 DNA polymerase[44] and barcoded primers for 12 cycles. The PCR product was purified via a 1.5× SPRI clean-up (Agencourt) and checked for a characteristic nucleosome banding pattern using TapeStation (Agilent). Samples were sequenced on a NextSeq 500 (Illumina) using the v2.5 75-cycle kit (single end).

ATAC-seq analysis

Single-end reads were aligned to the Gencode hg38 primary assembly[67] using Bowtie2 v.2.4.4[57]. We then used SAMtools v.1.9[68] to filter out alignments with low-mapping quality (MAPQ < 30) and subsequently to sort and index the filtered BAM files[68]. Read duplicates were removed using Picard v.4.1.8.1[69]. Peaks were called using MACS3 v.3.0.0[70] with default parameters (-g 2.7e9 -q 0.05).

To construct the union feature space ('union peaks') used for much of the downstream analyses, we began by performing intersections on pairs of biological replicate narrowPeak files using BEDTools v.2.29.0 (using bedtools intersect), keeping only those peaks found in both replicates[71]. After marking the shared peaks between replicates, we used bedtools merge to consolidate the biological replicates at each shared peak (at least 1 bp overlap). In this new peak BED file, each shared peak includes all sequence found under the peak in either of the biological replicates. Next, we took the union of each of these peak files (LTBR resting, LTBR stimulated, tNGFR resting, tNGFR stimulation); we combined any peaks with at least 1 bp overlap. Using the union peaks, we generated a peak read count matrix (union peaks × ATAC samples), in which each entry in the matrix corresponds to the number of reads overlapping that peak in the specified sample—we term this the per-peak ATAC matrix. The overlapping reads are taken directly from the BAM files (converted to BED) that provide an alignment for each sample. Thus, the matrix includes a column for each biological replicate. Although samples had minimal differences in aligned reads, we normalized each entry in the matrix by the number of reads that overlapped the TSS regions in each sample. In this manner, any difference in read or alignment depth between samples would be normalized appropriately. In addition to the per-peak ATAC matrix, we also constructed a per-gene ATAC matrix as follows: we assigned a gene's total ATAC reads as the sum of normalized reads from the per-peak ATAC matrix for all peaks within 3 kb of a gene's start or end coordinates.

We imported these two ATAC matrices (per-peak and per-gene) into R v.4.1.1 for gene and peak enrichment analysis using DESeq2 v.1.32.0 (Supplementary Tables 13, 14). For comparison between ATAC-seq and RNA-seq, we used a statistical threshold of adjusted *P* value < 0.05 and either $\log_2$-transformed fold change > 0 (for increases in ATAC or RNA) or $\log_2$-transformed fold change < 0 (for decreases in ATAC or RNA). For transcription factor-motif analysis we used ChromVAR v.1.14.0[72] as follows: For each of the test versus control conditions,

we constructed SummarizedExperiment objects using column and sample subsets of the per-peak matrix and the union feature space. We used the matchMotifs function to annotate transcription factor motifs. We computed enrichment deviations between test and control conditions using the computeDeviations function.

To produce read pile-up tracks at specific genomic loci, we pooled de-duplicated reads from biological replicates (BAM) using samtools merge. We converted these pooled-replicate BAM files to bigWig files by using the bamCoverage function from deeptools v.3.4.2 and setting the scaleFactor to the relative number of TSSs found in the pooled biological replicates compared to all other sample aggregates[73]. Using the bigWig files, read pileups were plotted with pyGenomeTracks v.3.6[74].

Finally, we performed *k*-means clustering on ATAC peaks near genes with increased chromatin accessibility. First, using DEseq2 on the ATAC per-gene matrix, we identified genes with $\log_2$-transformed fold change > 1 and adjusted *P* value < 0.05 (that is, genes with increased chromatin accessibility) in either of two comparisons: (1) LTBR stimulated versus tNGFR stimulated; (2) LTBR resting versus tNGFR resting. After identifying these genes, we isolated all accessibility peaks in the per-peak ATAC matrix within 3 kb of the gene body; this subset of peaks from the per-peak ATAC matrix was used as input for the clustering. Then, using deeptools (computeMatrix and plotHeatmap functions) on this subset of ATAC peaks, we performed *k*-means clustering with $k = 4$ clusters and 6 kb read windows.

Statistical analysis

Data between two groups were compared using a two-tailed unpaired Student's *t*-test or the Mann–Whitney test as appropriate for the type of data (depending on the normality of the distribution). Unless otherwise indicated, a *P* value less than or equal to 0.05 was considered statistically significant for all analyses, and not corrected for multiple comparisons. In cases in which multiple comparison corrections were necessary, we adjusted the *P* value using the Benjamini–Hochberg method. All group results are represented as mean ± s.e.m, if not stated otherwise. Statistical analyses were performed in Prism (GraphPad) and RStudio (Rstudio PBC). Flow cytometry data were analysed using FlowJo v.10.7.1 (Treestar).

Reporting summary

Further information on research design is available in the Nature Research Reporting Summary linked to this paper.

Data availability

Data from the ORF screen, OverCITE-seq, bulk RNA-seq and ATAC-seq have been deposited in the Gene Expression Omnibus (GEO) with accession number GSE193736. The following publicly available datasets have also been used in the study: DICE (https://dice-database.org/), Genotype-Tissue Expression Project v.8 (https://www.gtexportal.org/) and Single Cell Portal (https://singlecell.broadinstitute.org/single_cell/study/SCP424/single-cell-comparison-pbmc-data).

42. Lissina, A. et al. Protein kinase inhibitors substantially improve the physical detection of T-cells with peptide-MHC tetramers. *J. Immunol. Methods* **340**, 11–24 (2009).
43. Meier, J. A., Zhang, F. & Sanjana, N. E. GUIDES: sgRNA design for loss-of-function screens. *Nat. Methods* **14**, 831–832 (2017).
44. Liscovitch-Brauer, N. et al. Profiling the genetic determinants of chromatin accessibility with scalable single-cell CRISPR screens. *Nat. Biotechnol.* **39**, 1270–1277 (2021).
45. Dobin, A. et al. STAR: ultrafast universal RNA-seq aligner. *Bioinformatics* **29**, 15–21 (2013).
46. Legut, M. et al. High-throughput screens of PAM-flexible Cas9 variants for gene knockout and transcriptional modulation. *Cell Rep.* **30**, 2859–2868 (2020).
47. Langmead, B., Trapnell, C., Pop, M. & Salzberg, S. L. Ultrafast and memory-efficient alignment of short DNA sequences to the human genome. *Genome Biol.* **10**, R25 (2009).
48. Martin, M. Cutadapt removes adapter sequences from high-throughput sequencing reads. *EMBnet j.* **17**, 10 (2011).
49. Wang, B. et al. Integrative analysis of pooled CRISPR genetic screens using MAGeCKFlute. *Nat. Protoc.* **14**, 756–780 (2019).
50. Love, M. I., Huber, W. & Anders, S. Moderated estimation of fold change and dispersion for RNA-seq data with DESeq2. *Genome Biol.* **15**, 550 (2014).
51. Alexa, A. & Rahnenfuhrer, J. topGO: Enrichment Analysis for Gene Ontology R package v.2.46.0 (Bioconductor, 2021).
52. Rambaldi, D., Pece, S. & Di Fiore, P. P. flowFit: a Bioconductor package to estimate proliferation in cell-tracking dye studies. *Bioinformatics* **30**, 2060–2065 (2014).
53. Wessels, H.-H. et al. Massively parallel Cas13 screens reveal principles for guide RNA design. *Nat. Biotechnol.* **38**, 722–727 (2020).
54. Guedan, S., Calderon, H., Posey, A. D. & Maus, M. V. Engineering and design of chimeric antigen receptors. *Mol. Ther. Methods Clin. Dev.* **12**, 145–156 (2019).
55. Melsted, P. et al. Modular, efficient and constant-memory single-cell RNA-seq preprocessing. *Nat. Biotechnol.* **39**, 813–818 (2021).
56. Melsted, P., Ntranos, V. & Pachter, L. The barcode, UMI, set format and BUStools. *Bioinformatics* **35**, 4472–4473 (2019).
57. Langmead, B. & Salzberg, S. L. Fast gapped-read alignment with Bowtie 2. *Nat. Methods* **9**, 357–359 (2012).
58. Stoeckius, M. et al. Cell Hashing with barcoded antibodies enables multiplexing and doublet detection for single cell genomics. *Genome Biol.* **19**, 224 (2018).
59. McGinnis, C. S. et al. MULTI-seq: sample multiplexing for single-cell RNA sequencing using lipid-tagged indices. *Nat. Methods* **16**, 619–626 (2019).
60. Hao, Y. et al. Integrated analysis of multimodal single-cell data. *Cell* **184**, 3573–3587 (2021).
61. Chung, N. C. & Storey, J. D. Statistical significance of variables driving systematic variation in high-dimensional data. *Bioinformatics* **31**, 545–554 (2015).
62. Becht, E. et al. Dimensionality reduction for visualizing single-cell data using UMAP. *Nat. Biotechnol.* **37**, 88–44 (2018).
63. Storey, J. D. & Tibshirani, R. Statistical significance for genomewide studies. *Proc. Natl Acad. Sci. USA* **100**, 9440–9445 (2003).
64. Pallares, L. F., Picard, S. & Ayroles, J. F. TM3'seq: a tagmentation-mediated 3' sequencing approach for improving scalability of RNAseq experiments. *G3* **10**, 143–150 (2020).
65. Yates, A. D. et al. Ensembl 2020. *Nucleic Acids Res.* **48**, D682–D688 (2019).
66. Soneson, C., Love, M. I. & Robinson, M. D. Differential analyses for RNA-seq: transcript-level estimates improve gene-level inferences. *F1000Res.* **4**, 1521 (2015).
67. Schneider, V. A. et al. Evaluation of GRCh38 and de novo haploid genome assemblies demonstrates the enduring quality of the reference assembly. *Genome Res.* **27**, 849–864 (2017).
68. Li, H. et al. The Sequence Alignment/Map format and SAMtools. *Bioinformatics* **25**, 2078–2079 (2009).
69. Broad Institute. Picard Toolkit https://broadinstitute.github.io/picard/ (Broad Institute, GitHub Repository, 2019).
70. Zhang, Y. et al. Model-based analysis of ChIP–seq (MACS). *Genome Biol.* **9**, R137 (2008).
71. Quinlan, A. R. & Hall, I. M. BEDTools: a flexible suite of utilities for comparing genomic features. *Bioinformatics* **26**, 841–842 (2010).
72. Schep, A. N., Wu, B., Buenrostro, J. D. & Greenleaf, W. J. chromVAR: inferring transcription-factor-associated accessibility from single-cell epigenomic data. *Nat. Methods* **14**, 975–978 (2017).
73. Ramírez, F., Dündar, F., Diehl, S., Grüning, B. A. & Manke, T. deepTools: a flexible platform for exploring deep-sequencing data. *Nucleic Acids Res.* **42**, W187–W191 (2014).
74. Lopez-Delisle, L. et al. pyGenomeTracks: reproducible plots for multivariate genomic datasets. *Bioinformatics* **37**, 422–423 (2021).
75. GTEx Consortium. The GTEx Consortium atlas of genetic regulatory effects across human tissues. *Science* **369**, 1318–1330 (2020).
76. Ding, J. et al. Systematic comparative analysis of single cell and single-nucleus RNA-sequencing methods. *Nat. Biotechnol.* **38**, 737–746 (2020).

Acknowledgements We thank the entire Sanjana laboratory for support and advice, and the New York University (NYU) Biology Genomics Core for sequencing resources. M.L. is supported by the Hope Funds for Cancer Research postdoctoral fellowship; Z.G. is supported by the National Institutes of Health (NIH) T32 Training Grant (GM136573); and N.E.S. is supported by NYU and NYGC start-up funds, NIH–NHGRI (R00HG008171 and DP2HG010099), NIH–NCI (R01CA218668), DARPA (D18AP00053), the Cancer Research Institute and the Sidney Kimmel Foundation.

Author contributions M.L. and N.E.S. designed the study. M.L. performed the screens and validation experiments (including single-cell and CAR work) and analysed data. Z.G. assisted with screens and single-cell data analysis. Z.G., M.G. and X.X. assisted with lentivirus production, T cell transduction, cell culture and flow cytometry. Z.D. and L.L. performed western blots. J.A.R. assisted with screen and ATAC-seq analyses. C.L. assisted with ATAC-seq. E.P.M., S.H. and P.S. assisted with single-cell experiments. T.D. contributed reagents. C.D. contributed patient samples. M.L. and N.E.S. wrote the manuscript with input from all authors. N.E.S. supervised the study.

Competing interests The New York Genome Center and New York University have applied for patents relating to the screening methods, identified targets and OverCITE-seq. C.D. receives research funding from Fate Therapeutics and Bristol Myers Squibb. N.E.S. is an adviser to Vertex and Qiagen.

Additional information

Supplementary information The online version contains supplementary material available at https://doi.org/10.1038/s41586-022-04494-7.

Correspondence and requests for materials should be addressed to Mateusz Legut or Neville E. Sanjana.

Peer review information *Nature* thanks William Haining, Benedict Seddon and Elena Sotillo for their contribution to the peer review of this work.

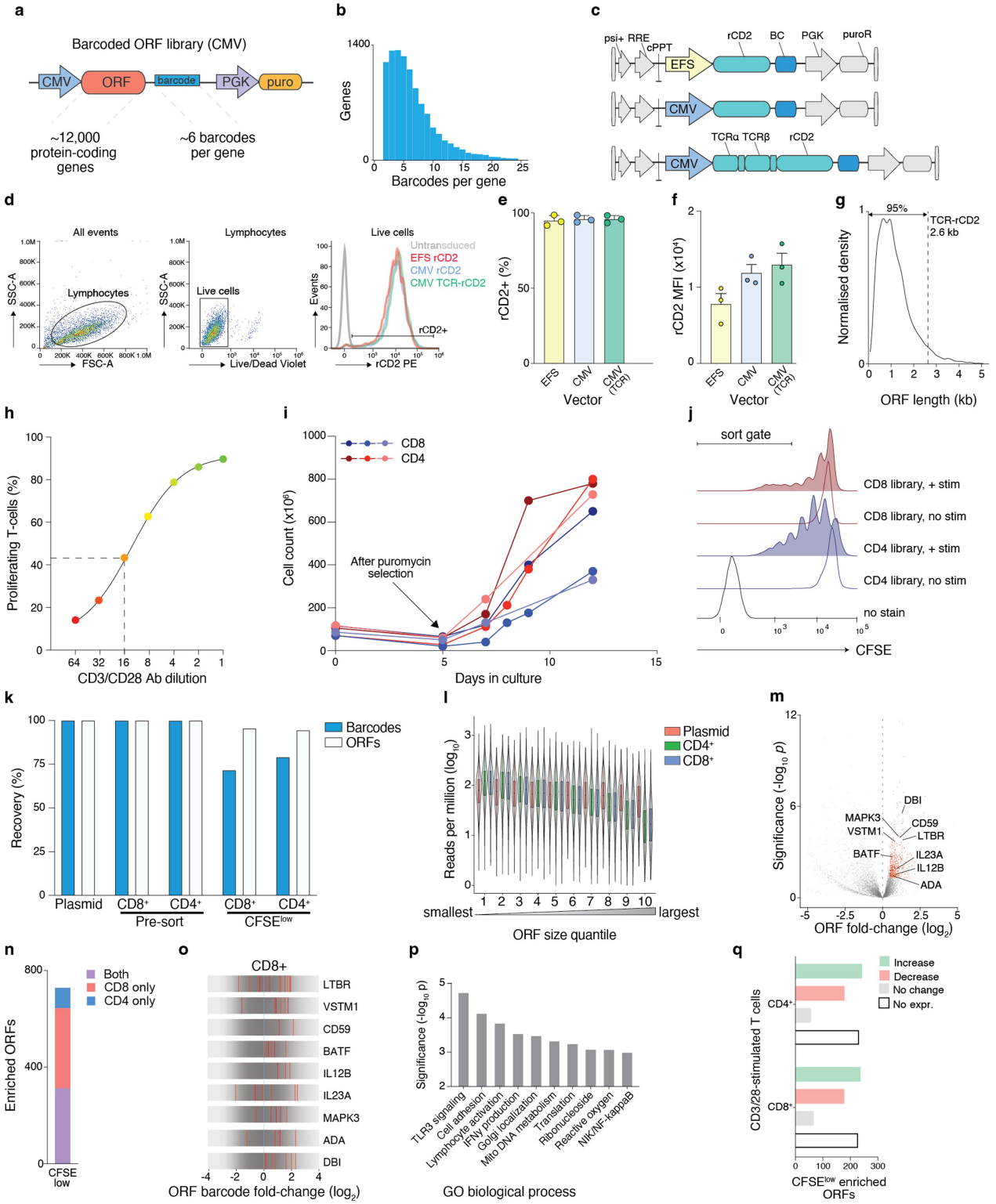

Extended Data Fig. 1 | See next page for caption.

Extended Data Fig. 1 | Design of the human ORF library screen in primary T cells. a, Barcoded vector design for ORF overexpression. **b**, Distribution of the number of barcodes per ORF in the library. **c**, Vector design for quantifying the effect of different promoters and ORF insert sizes on lentiviral transduction efficiency. EFS – elongation factor-1α short promoter, CMV – cytomegalovirus promoter, PGK – phosphoglycerate kinase-1 promoter. **d**, Sequential gating strategy and representative histograms of cells transduced with marker gene rat CD2 under different promoters. **e**, Percentage of positive cells and **f**, mean fluorescence intensity (MFI) of rat CD2 (rCD2) expressed from the EFS and CMV promoters, following puromycin selection of transduced primary CD4+ T cells. Each data point indicates individual transduction (n = 3 biological replicates). Error bars are SEM. **g**, Distribution of ORF sizes in the genome-scale library. The size of TCR-rCD2 construct tested in panels *e* and *f* is marked. **h**, Titration of CD3/CD28 antibodies. T cells were labelled with CFSE, stimulated and incubated for 4 days. Gate for proliferating T cells was set to include cells that proliferated at least twice (third CFSE peak). **i**, Expansion of T cells from three healthy donors transduced with the ORF library. **j**, Representative CFSE profile of restimulated CD8+ and CD4+ T cells before the sort. The $CFSE^{low}$ sort gate is marked. **k**, Recovery of individual barcodes or corresponding ORFs in transduced T cells and plasmid used for lentivirus production. Respective samples from three donors were computationally pooled together at equal number of reads prior to counting how many barcodes or ORFs were present with a minimum of one read. **l**, Distribution of reads corresponding to ORFs of different sizes. ORFs were assigned to ten quantiles based on their size, with Q1 being smallest size and Q10 being the largest size (n = 1,161 ORFs per quantile). Box shows 25–75 percentile with a line at the median; whiskers extend to 1.5 × interquartile range. **m**, Enrichment of genes in both $CFSE^{low}$ CD4+ and CD8+ T cells, calculated by collapsing individual barcodes into corresponding genes. Significantly enriched genes ($\log_2$ fold change higher than 0.5 and adjusted p-value lower than 0.05) are marked in red. Immune response genes of interest are marked. **n**, Overlap of significantly enriched genes from panel *m* in individual screen populations (CD4+, CD8+) analysed separately. **o**, Normalized enrichment of individual barcodes for indicated genes in the CD8+ screen. **p**, GO biological processes for significantly enriched genes in panel *m*. **q**, Overlap of significantly enriched genes with differentially expressed genes between CD3/CD28 stimulated and naive T cells[41].

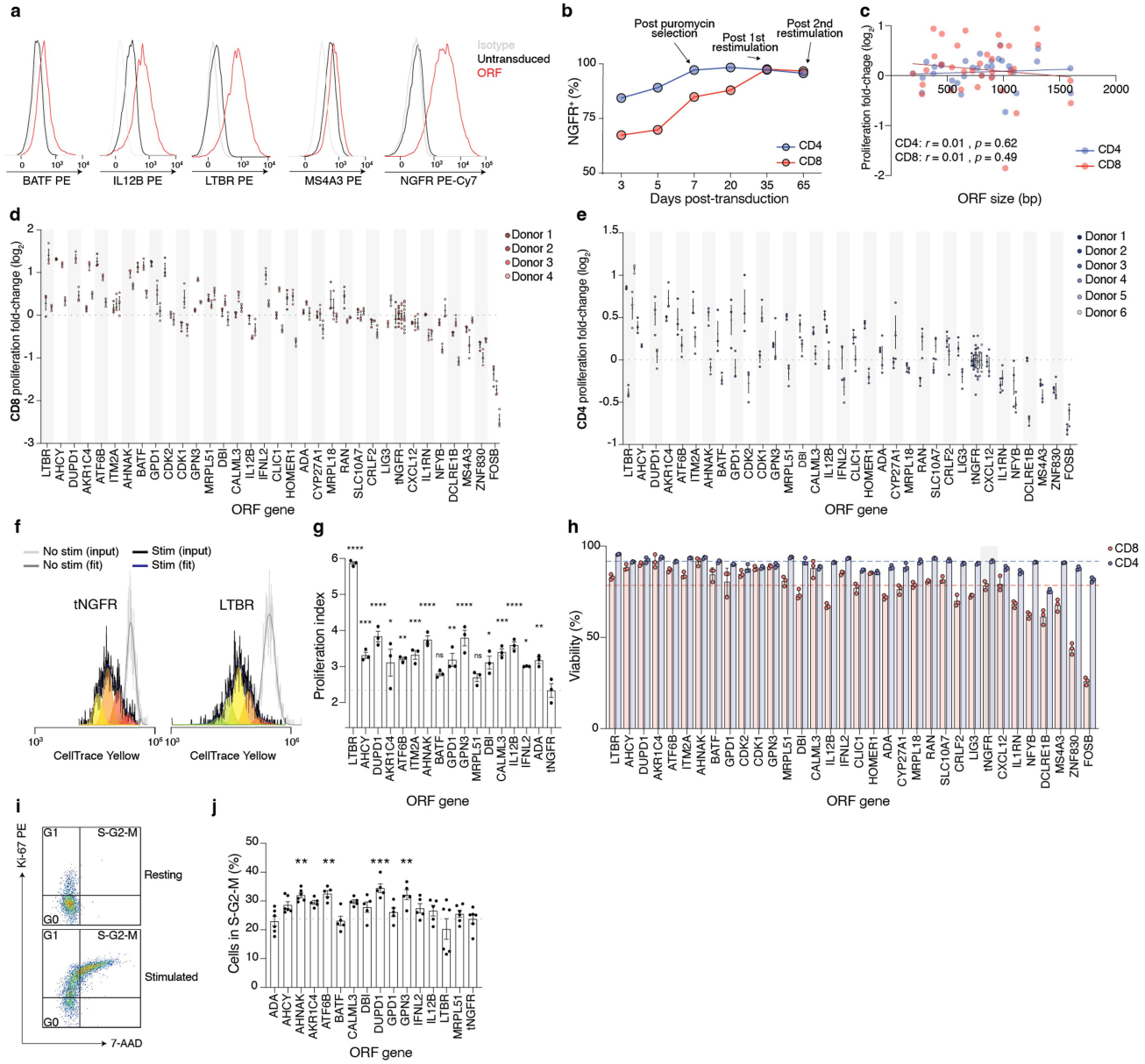

Extended Data Fig. 2 | Overexpression of select ORFs in screen-independent donors. a, Histograms of selected ORF expression in T cells after puromycin selection. **b**, Quantification of tNGFR expression in transduced CD4+ and CD8+ T cells. Puromycin selection was complete after 7 days post transduction. To maintain T cells in culture, they were restimulated with CD3/CD28 on days 21 and 42. **c**, Correlation between ORF sizes and changes in proliferation relative to tNGFR. Mean $\log_2$ fold-changes are shown. **d**, Proliferation of restimulated CD8+ or **e**, CD4+ T cells relative to tNGFR in individual donors ($n = 3$ biological replicates). Mean and SEM are shown. **f**, **g**, Proliferation of T cells transduced with ORFs that significantly improved T cell proliferation (see Fig. 2c) measured by dilution of CellTrace Yellow. Representative CellTrace Yellow histograms and fitted distributions (**f**) as well as quantifications of the proliferation index (**g**) are shown ($n = 3$ biological replicates). *P* values: < 0.0001, 0.0008, < 0.0001, 0.011, 0.0031, 0.0007, < 0.0001, 0.28, 0.004, < 0.0001, 0.58, 0.01, 0.0003, < 0.0001, 0.036, 0.0049 (left to right). **h**, Viability of ORF-transduced T cells 4 days after CD3/CD28 restimulation. Representative data from one donor (out of 4 donors tested) are shown ($n = 3$ biological replicates). **i**, **j**, Cell cycle analysis of T cells stimulated with CD3/CD28 for 24 h. Gating was performed based on isotype and fluorescence minus one controls. Representative gating (**i**) as well as (**j**) quantification of cells in the S-G2-M phases (for stimulated T cells) are shown ($n = 6$ biological replicates from two donors). *P* values: 1, 0.29, 0.0065, 0.17, 0.0051, 1, 0.13, 0.55, 0.0004, 0.98, 0.0088, 0.68, 0.91, 0.7, 1 (left to right). Statistical significance for panels **g** and **j**: one way ANOVA with Dunnett's multiple comparisons test $^{*}p < 0.05$, $^{**}p < 0.01$, $^{***}p < 0.001$, $^{****}p < 0.0001$. Error bars indicate SEM.

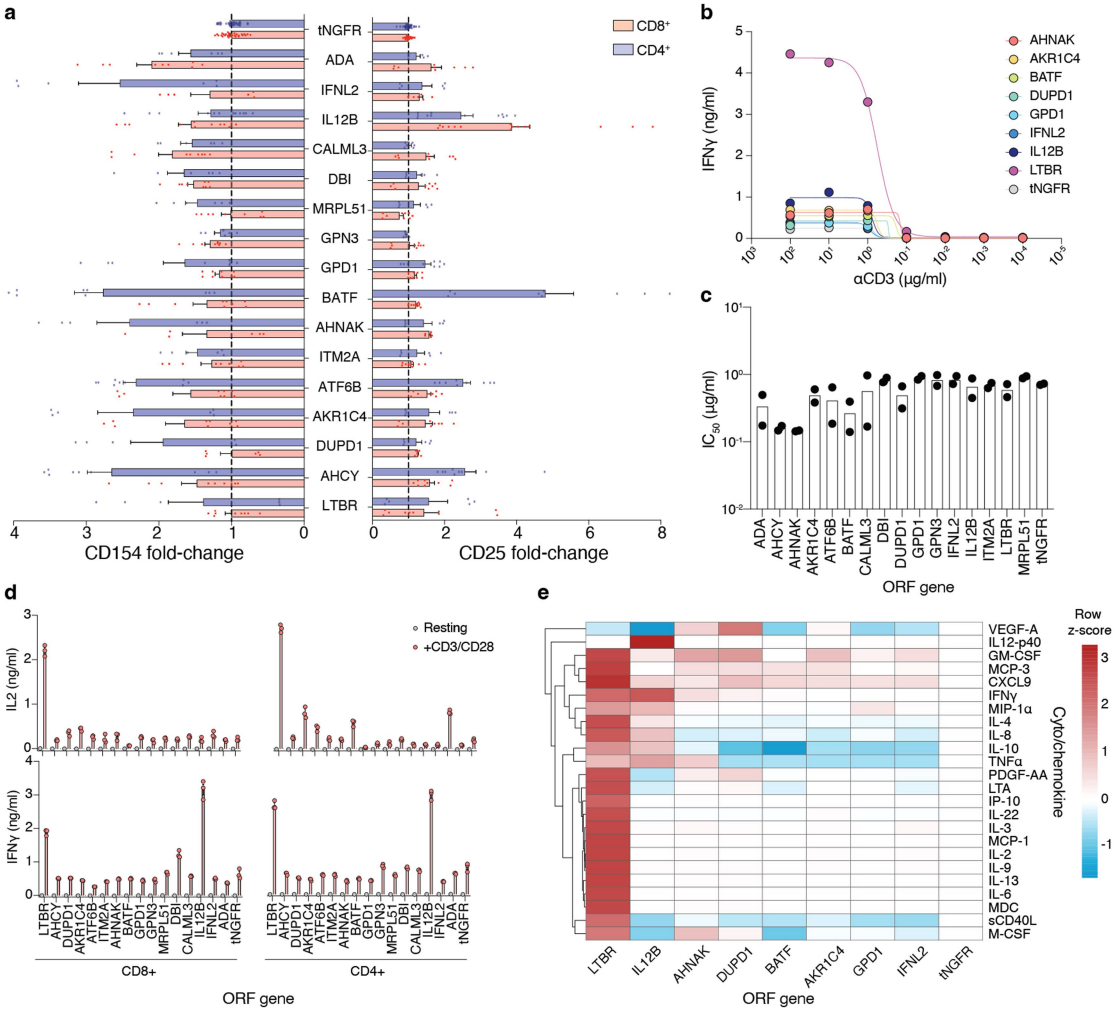

Extended Data Fig. 3 | Functional response of ORF-overexpressing T cells. **a**, Quantitative expression of CD25 or CD154 following restimulation. A minimum of two donors was tested in triplicate per gene. Only genes that significant increase T cell proliferation in CD4+, CD8+ or both T cell subsets are shown. Mean and SEM are shown. **b**, **c**, Sensitivity to antigen dose. T cells were incubated with indicated anti-CD3 antibody concentrations for 24 h and the amount of secreted IFNγ was quantified. Representative dose-response curve fitting (**b**) and IC_{50} quantifications (**c**) are shown ($n = 2$ biological replicates). **d**, Quantification of secreted IL-2 and IFNγ in T cells incubated alone or with CD3/CD28 antibodies for 24 h. Representative data from one out of four donors ($n = 3$ biological replicates) are shown. **e**, Multiplexed quantification of selected secreted cytokines and chemokines by ORF-transduced T cells after 24 h of CD3/CD28 stimulation. Means of duplicate measurements (from independent samples) *z*-score normalized to tNGFR are shown. Absolute quantities of secreted cytokines and chemokines in stimulated and resting T cells are shown in Supplementary Table 7.

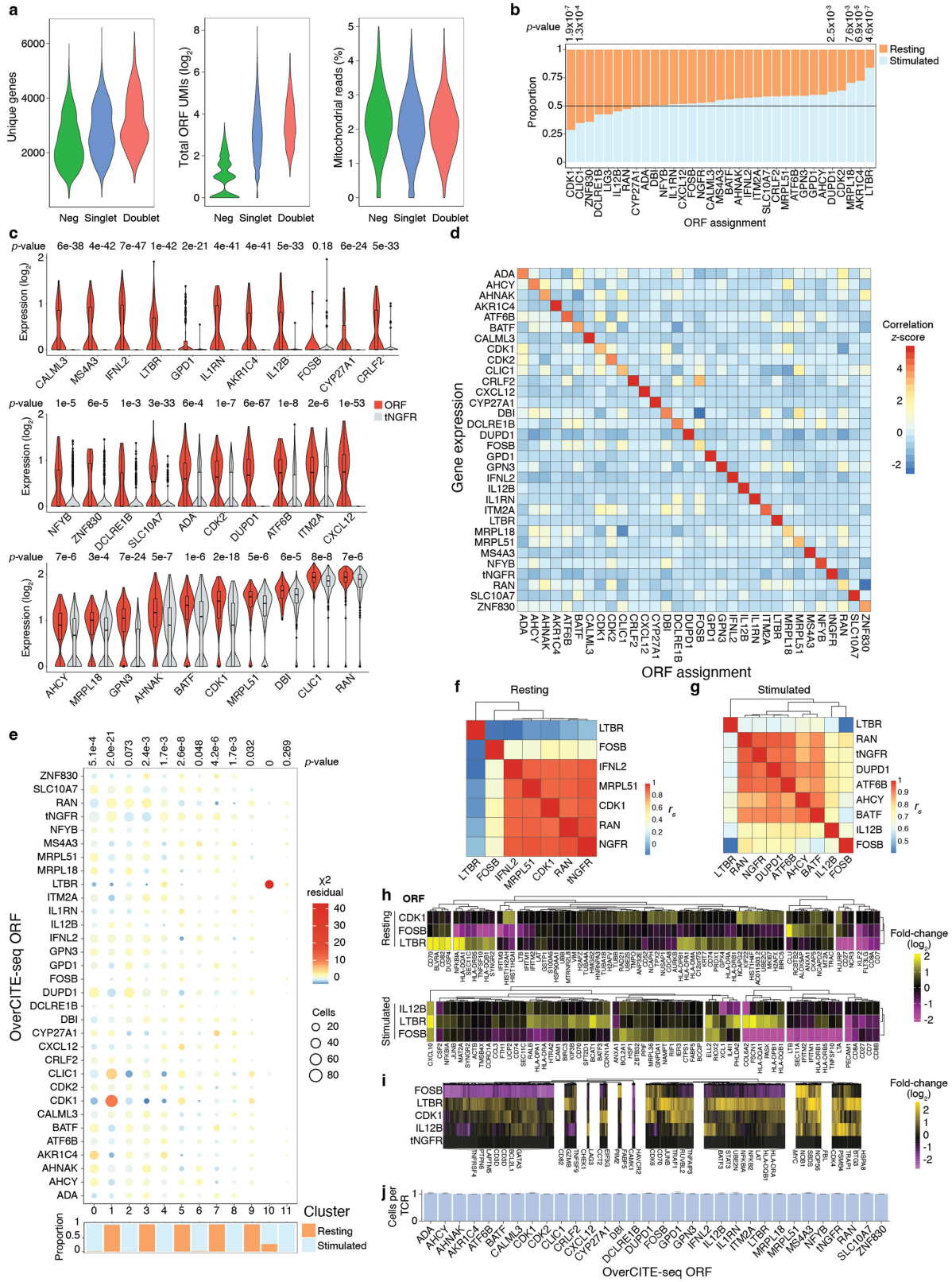

Extended Data Fig. 4 | See next page for caption.

Extended Data Fig. 4 | OverCITE-seq identifies ORFs and their transcriptional effects. a, Quality parameters of cells as identified by gel bead barcodes. Negative, singlets and doublets are assigned based on cell hashing. **b**, Proportion of stimulated and resting T cells among cells assigned to each ORF. Chi-squared test *p*-values are shown for ORFs with significantly shifted (uneven) distributions of stimulated and rested cells. **c**, Cell-cycle corrected scaled expression of the overexpressed gene in the cells transduced with the respective ORF and negative control (tNGFR). Two-sided Wilcoxon test *p*-values shown above the violin plots indicate the statistical significance of gene expression level between specific ORF and tNGFR-transduced T cells. Box shows 25–75 percentile with a line at the median; whiskers extend to maximum and minimum values. $N = 71$ (ADA), 147 (AHCY), 190 (AHNAK), 119 (AKR1C4), 124 (ATF6B), 179 (BATF), 137 (CALML3), 189 (CDK1), 129 (CDK2), 236 (CLIC1), 84 (CRLF2), 91 (CXCL12), 88 (CYP27A1), 129 (DBI), 26 (DCLRE1B), 261 (DUPD1), 25 (FOSB), 119 (GPD1), 124 (GPN3), 199 (IFNL2), 60 (IL12B), 70 (IL1RN), 156 (ITM2A), 74 (LTBR), 88 (MRPL18), 167 (MRPL51), 107 (MS4A3), 69 (NFYB), 355 (NGFR), 261 (RAN), 182 (SLC10A7), and 56 (ZNF830) single cells. **d**, Expression of all ORF genes by cells assigned each ORF. Each row is z-score normalized. **e**, Distribution of individual ORF frequencies in clusters. Numbers of ORF cells and the chi-squared test residuals are displayed. Chi-squared test *p*-values indicating whether ORF distribution in each cluster significantly differs from overall ORF distribution are shown on top of the plot. Proportions of stimulated and resting T cells in each cluster are shown underneath the cluster label. **f**, **g**, Spearman correlations between transcriptional profiles of selected ORF cells in resting (**f**) and stimulated (**g**) populations. **h**, Fold change of top differentially expressed genes between cells with the indicated ORFs in resting and stimulated T cells. For each condition, the ORFs with the strongest transcriptional changes (compared to tNGFR cells) are shown. **i**, Differential gene expression in stimulated ORF T cells compared to resting T cells. Genes with significant expression changes in at least one ORF are shown (DESeq2 adjusted $p < 0.05$). For all genes, we display $\log_2$ fold-change of each ORF (stimulated) to tNGFR (resting), normalized to $\log_2$ fold-change of tNGFR (stimulated) to tNGFR (resting). Genes of interest in each cluster are labelled. **j**, Mean TCR clonotype diversity in ORF cells.

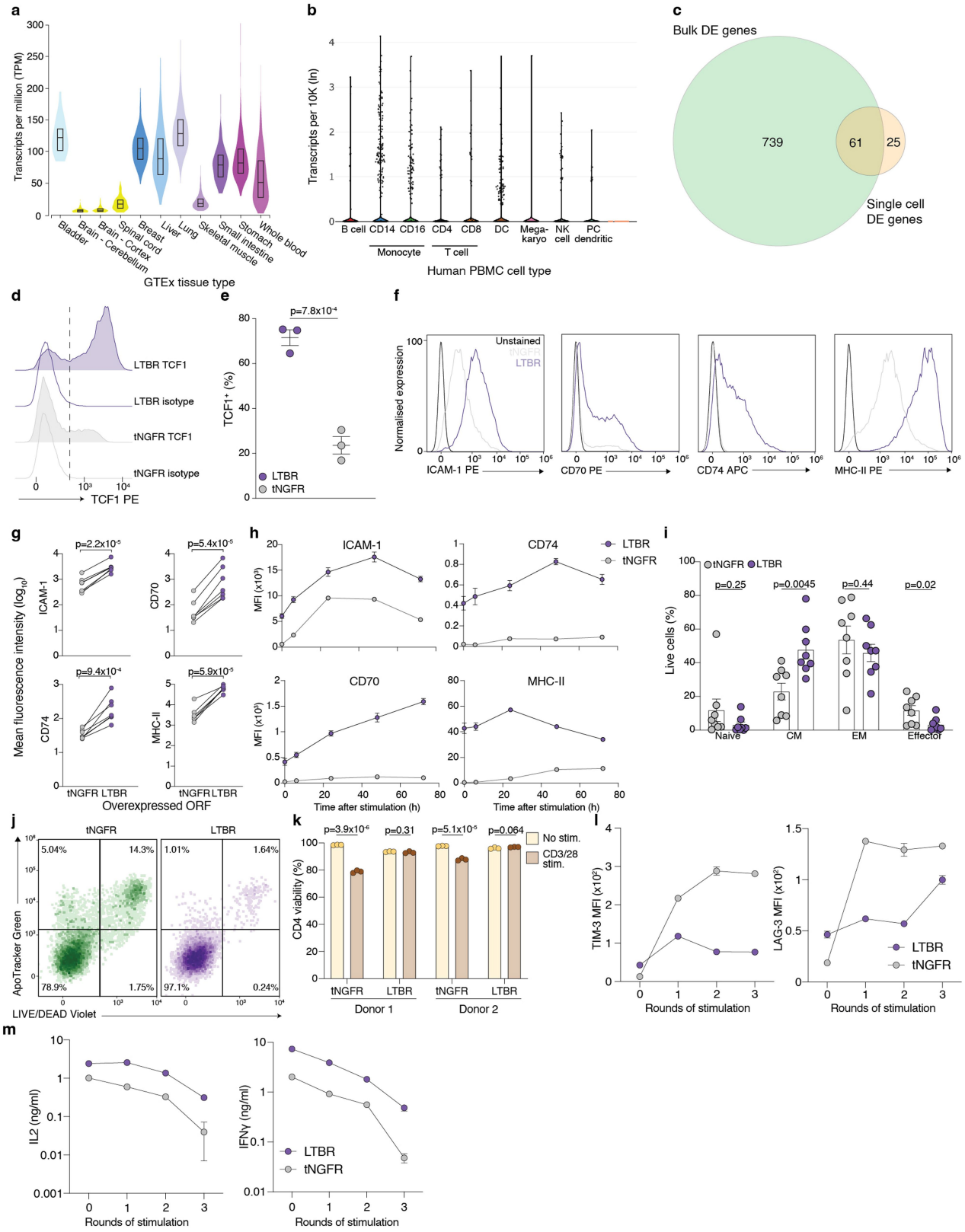

Extended Data Fig. 5 | See next page for caption.

Extended Data Fig. 5 | Functional analysis of *LTBR* overexpression in T cells. **a**, *LTBR* expression in the indicated human primary tissues from the Genotype-Tissue Expression (GTEx) project v8[75] ($n = 948$ donors). Box shows 25–75 percentile with a line at the median. **b**, *LTBR* expression in peripheral blood mononuclear cells (PBMCs) from 31,021 cells from 2 donors[76]. Cell types indicated are derived from Harmony tSNE clustering of single-cell transcriptomes. **c**, Overlap between significantly upregulated genes in LTBR cells compared to tNGFR cells identified in single-cell or bulk RNA-seq. **d**, **e**, TCF1 expression in LTBR or tNGFR transduced T cells. **d**, Representative histograms of TCF1 expression and the gate for TCF1+ cells (dashed line) are shown, as well as **e**, quantification of TCF1+ cells ($n = 3$ biological replicates). **f**–**h**, ICAM-1, CD70, CD74, and MHC-II expression in LTBR and tNGFR T cells. Representative histograms (**f**), quantification (**g**) in $n = 3$ donors (CD8+) or $n = 4$ donors (CD4+) and time course (**h**) of expression in LTBR and tNGFR cells after CD3/CD28 stimulation ($n = 3$ biological replicates). **i**, Differentiation phenotype of NGFR and LTBR transduced T cells ($n = 4$ donors, CD4+ and CD8+ separately). CM: Central memory. EM: Effector memory. Differentiation was defined based on CD45RO and CCR7 expression (naïve: $CD45RO^{neg}\,CCR7^{+}$, CM: $CD45RO^{+}\,CCR7^{+}$, EM: $CD45RO^{+}\,CCR7^{neg}$, effector $CD45RO^{neg}\,CCR7^{neg}$). **j**, Representative dot plots of T cell viability after CD3/CD28 stimulation. Viable cells are in the lower left quadrant. **k**, Cell viability of CD4+ T cells transduced with LTBR or tNGFR lentivirus, either restimulated with CD3/CD28 for four days or left unstimulated ($n = 2$ donors with 3 biological replicates each). **l**, **m**, LTBR and tNGFR cells were stimulated with a 3:1 excess of CD3/CD28 beads every three days for up to three rounds of stimulation. Following repeated stimulation, expression of TIM-3 and LAG-3 (**l**) was measured in resting cells, and secretion of IFNγ and IL2 (**m**) was measured in restimulated cells ($n = 3$ biological replicates). Statistical significance for panels **e**, **i**, and **k**: two-sided unpaired *t*-test; for panel **g**: two-sided paired *t*-test. Error bars indicate SEM.

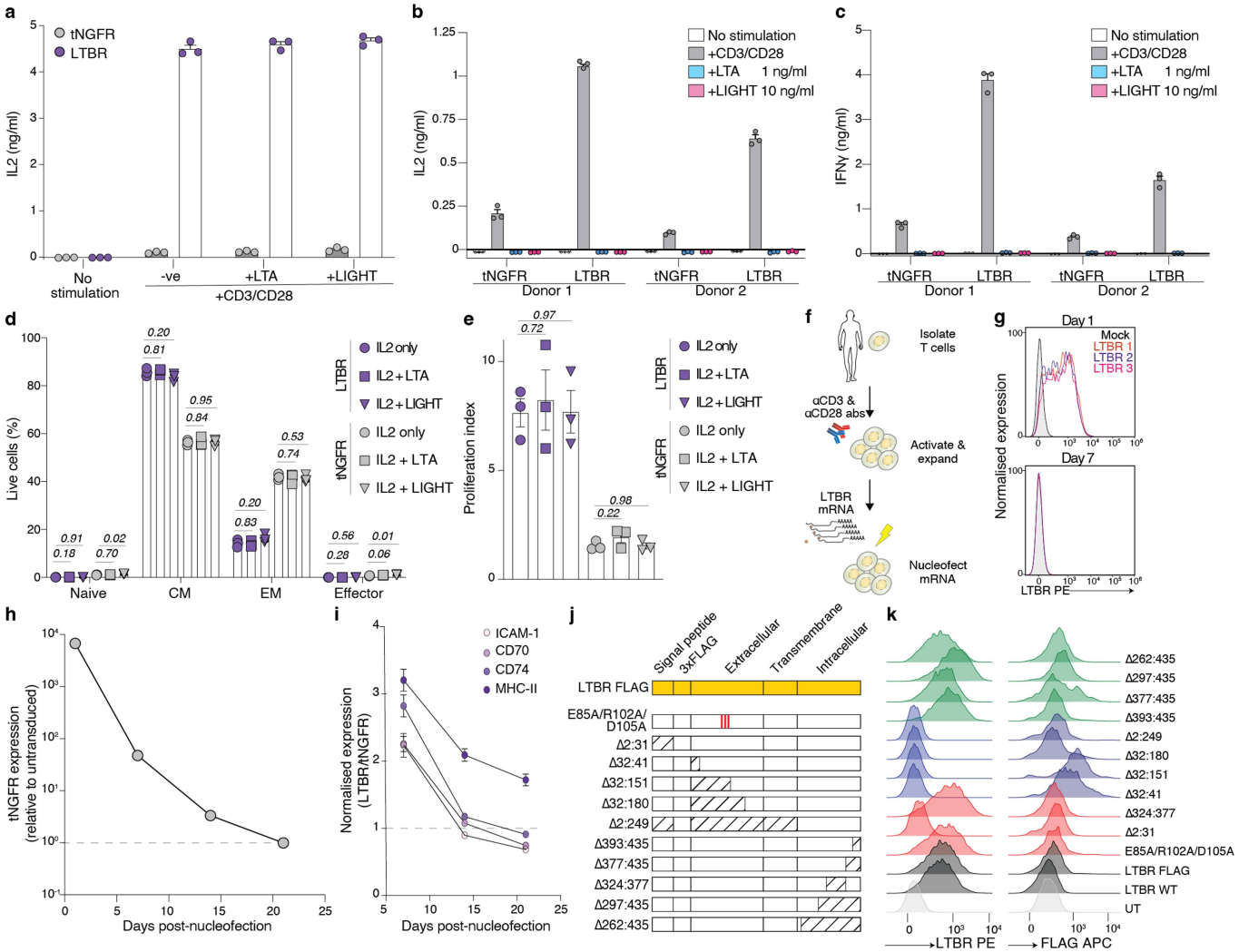

Extended Data Fig. 6 | LTBR ligands and expression of LTBR via mRNA or with deletion and point mutants. a, IL2 secretion after 24 h stimulation with CD3/CD28 antibodies. Where indicated, recombinant soluble LTA (1 ng/mL) or LIGHT (10 ng/mL) were added together with CD3/CD28 antibodies. CD4+ T cells from one donor were tested in triplicate. **b**, **c**, CD4+ and CD8+ T cells from two donors were co-incubated for 24 h with CD3/CD28 antibodies or recombinant soluble LTA or LIGHT and then IL2 (**b**) and IFNγ (**c**) were measured. ($n = 3$ biological replicates). **d**, **e**, Differentiation phenotype (**d**) or proliferation (**e**) after restimulation of tNGFR and LTBR transduced T cells ($n = 3$ biological replicates) incubated either with IL2 alone or with LTA (1 ng/mL) or LIGHT (10 ng/mL) for the duration of culture. CM: Central memory. EM: Effector memory. Unpaired two-sided *t*-test *p* values are shown. **f**–**i**, Transient LTBR or tNGFR expression via mRNA nucleofection (**f**). T cells were either nucleofected with LTBR or tNGFR mRNA ($n = 3$ biological replicates), and the surface expression of LTBR (**g**), tNGFR (**h**) or four genes upregulated in LTBR cells (**i**) was monitored over 21 days. At each timepoint the expression of target genes was normalized to matched tNGFR control. **j**, Schematic representation of FLAG-tagged LTBR mutants. **k**, LTBR and FLAG expression in T cells transduced with LTBR mutants. Error bars indicate SEM.

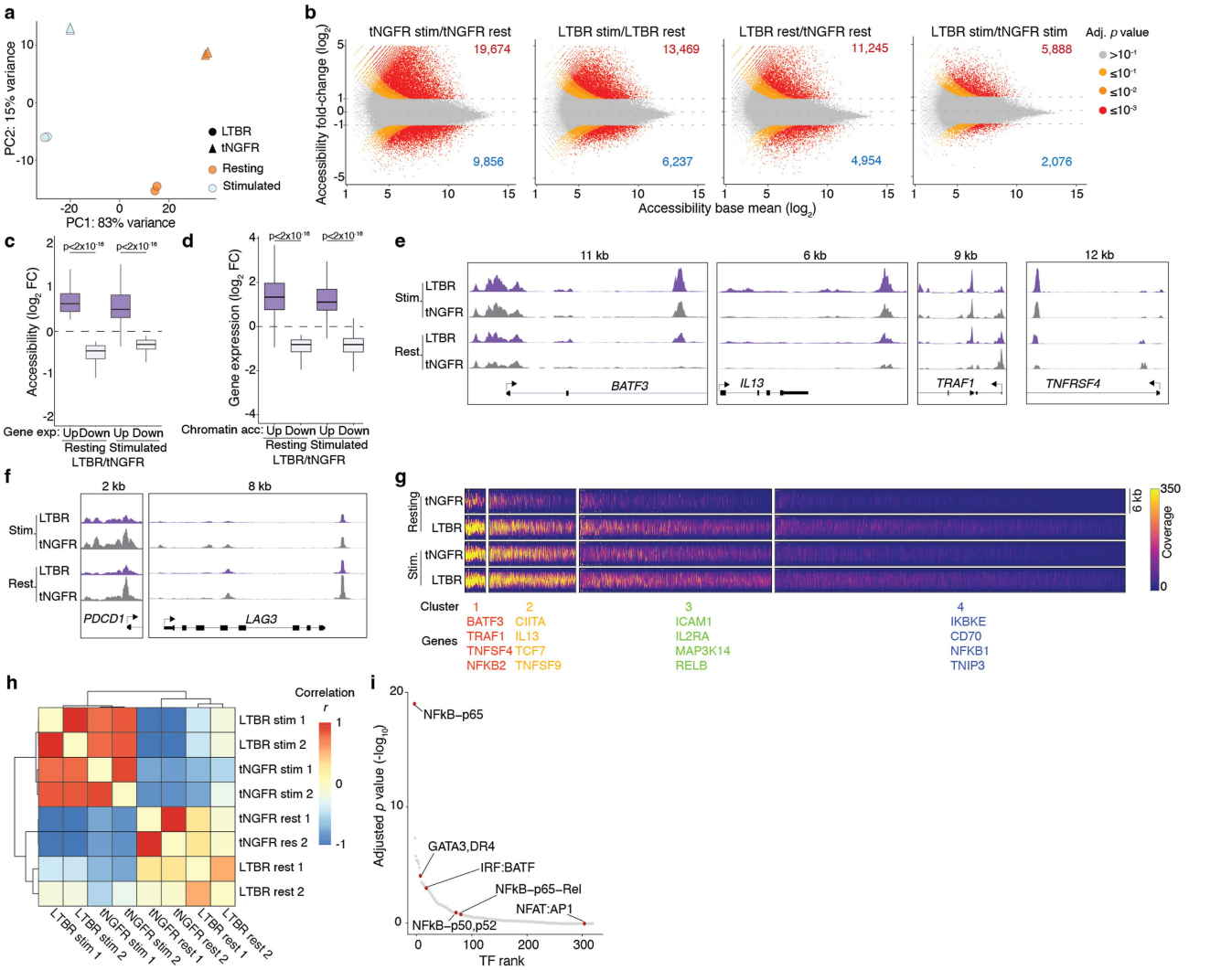

Extended Data Fig. 7 | Chromatin accessibility in LTBR T cells. a, Principal component (PC) analysis of global accessible chromatin regions of LTBR and tNGFR T cells, either resting or stimulated with CD3/CD28 for 24 h. **b**, Differentially accessible chromatin regions between stimulated and resting tNGFR, stimulated and resting LTBR, resting LTBR and resting tNGFR, and stimulated LTBR and stimulated tNGFR. Numbers of peaks gained/lost are shown (using absolute $\log_2$ fold change of 1 and adjusted p value < 0.1 as cut-off). **c**, **d**, Changes in chromatin accessibility (**c**) for differentially expressed (adjusted $p < 0.05$) genes or in gene expression (**d**) for differentially accessible (adjusted $p < 0.05$) regions. Two-sided t-test p values are shown. Box shows 25–75 percentile with a line at the median; whiskers extend to 1.5 × interquartile range. $N = 614$ genes (**c**) or genomic regions (**d**). **e**, **f**, Chromatin accessibility profiles at loci more (**e**) or less open (**f**) in LTBR compared to tNGFR cells, resting or stimulated for 24 h. The y-axis represents normalized reads (scale: 0–860 for *BATF3*, 0–1950 for *IL13*, 0–1230 for *TRAF1*, 0–1000 for *TNFSF4*, 0–300 for *PDCD1*, 0–2350 for *LAG3*). **g**, Chromatin accessibility in resting or stimulated LTBR and tNGFR cells. Each row represents a peak significantly enriched in LTBR over matched tNGFR control ($\log_2$ fold change > 1, DESeq2 adjusted p value < 0.05). Peaks were clustered using k-means clustering and selected genes at/near peaks from each cluster are indicated. **h**, Correlations for each ATAC sample (biological replicate) based on the bias-corrected deviations. **i**, Top transcription factor (TF) motifs enriched in the differentially accessible chromatin regions in resting LTBR cells compared to resting tNGFR cells.

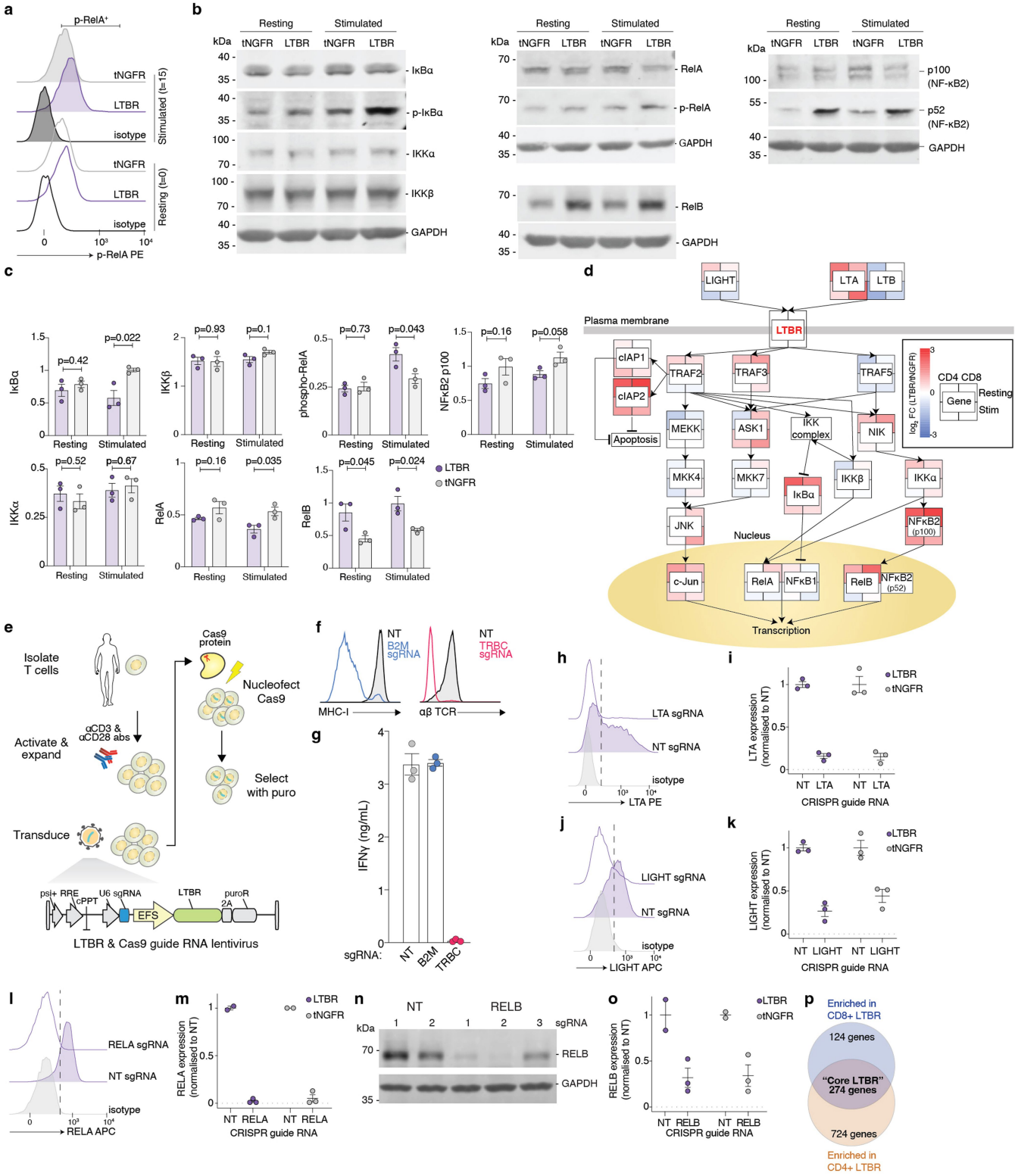

Extended Data Fig. 8 | See next page for caption.

Extended Data Fig. 8 | Proteomic and functional genomic assays of NF-κB activation. a, Phospho-RELA staining by intracellular flow cytometry in LTBR and tNGFR cells. Gating for identification of phospho-RELA+ cells is shown. **b**, **c**, Western blot quantification of key proteins in the NF-κB pathway in LTBR and tNGFR cells, resting or stimulated with CD3/CD28 for 15 min. Representative gels (**b**) or quantification of band intensity relative to GAPHD (**c**) are shown ($n = 3$ biological replicates). Unpaired two-sided *t* test *p* values are shown. **d**, Representation of the LTBR signalling pathway. Each gene is coloured based on the differential expression in LTBR over matched tNGFR cells (CD4+ and CD8+ T cells, resting or stimulated for 24 h). **e**–**g**, Simultaneous gene knockout via CRISPR and ORF overexpression. T cells were transduced with a lentiviral vector co-expressing a single guide RNA (sgRNA) and the LTBR ORF. After transduction, Cas9 protein was delivered via nucleofection. **f**, Representative expression of target genes in LTBR cells co-expressing an sgRNA targeting *B2M*, an essential component of the MHC-I complex, or *TRBC1/2*, an essential component of the αβ TCR. **g**, Quantification of IFNγ after restimulation ($n = 3$ sgRNAs). **h**–**o**, Representative protein-level based quantification of gene knockout efficiency. Representative histograms (**h**, **j**, **l**) and quantification of relative expression levels of LTA, LIGHT, and RELA (**i**, **k**, **m**) are shown ($n = 3$ sgRNAs). Dashed lines represent gates used to enumerate cells expressing a given protein. Representative gel (**n**) and quantification of RELB expression (**o**) are shown ($n = 3$ sgRNAs for RELB and 2 non-targeting control sgRNAs). **p**, Identification of 274 genes identified as enriched in both CD4+ and CD8+ T cells transduced with LTBR over matched tNGFR controls ("core LTBR" genes). See Supplementary Fig. 1 for uncropped gel images. Error bars indicate SEM.

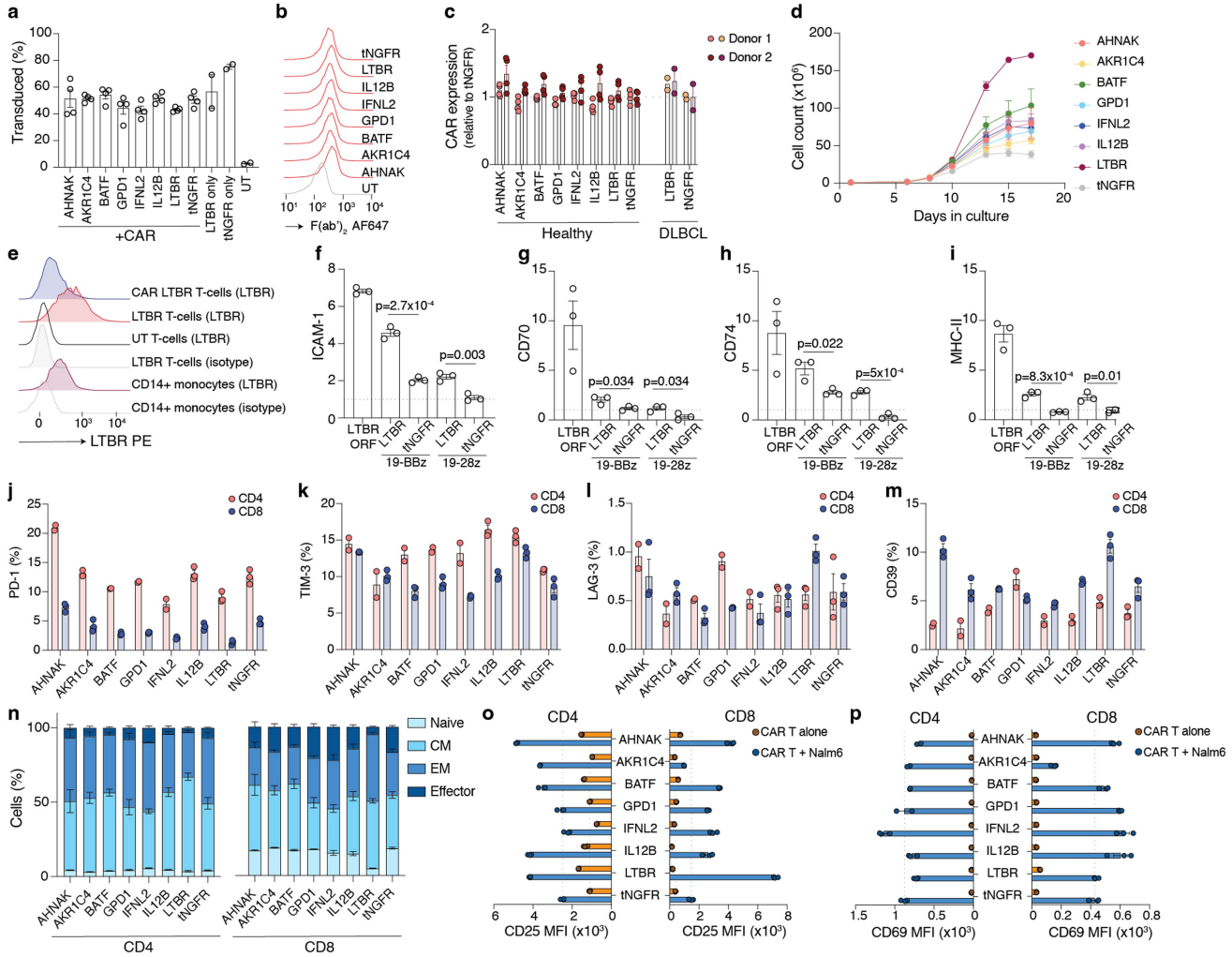

Extended Data Fig. 9 | Co-delivery of ORFs with CD19-targeting CARs. **a**, Transduction efficiency of CAR+ORF lentiviral vectors or ORF alone ($n = 4$ biological replicates). **b**, **c**, CAR expression level as determined by staining with anti-mouse Fab F(ab')$_2$. Representative histograms (**b**) and quantification of CAR expression relative to tNGFR (**c**) is shown for two healthy donors and two patients with diffuse large B cell lymphoma (DLBCL). **d**, Expansion curves of CAR+ORF transduced T cells ($n = 4$ biological replicates). **e**, LTBR expression in autologous CD14+ monocytes and T cells transduced with LTBR alone or CAR+LTBR. **f**–**I**, Expression of ICAM-1 (**f**), CD70 (**g**), CD74 (**h**) and MHC-II (**i**) by T cells transduced with LTBR ORF only, CAR + LTBR or CAR + tNGFR. All data are normalized to tNGFR only (no CAR). Unpaired two-sided *t* test *p* values are shown. **j**–**m**, Expression of exhaustion markers PD-1 (**j**), TIM-3 (**k**), LAG-3 (**l**) and CD39 (**m**) in CAR+ORF T cells. **n**, Differentiation phenotype of CAR+ORF T cells. CM: Central memory. EM: Effector memory. Differentiation was defined based on CD45RO and CCR7 expression (naïve: CD45RO^{neg} CCR7^{+}, CM: CD45RO^{+} CCR7^{+}, EM: CD45RO^{+} CCR7^{neg}, effector CD45RO^{neg} CCR7^{neg}). **o**, **p**, Expression of activation markers CD25 (**o**) and CD69 (**p**) in CAR+ORF T cells incubated alone or with Nalm6 cells for 24 h. Error bars indicate SEM. $N = 3$ biological replicates, unless indicated otherwise.

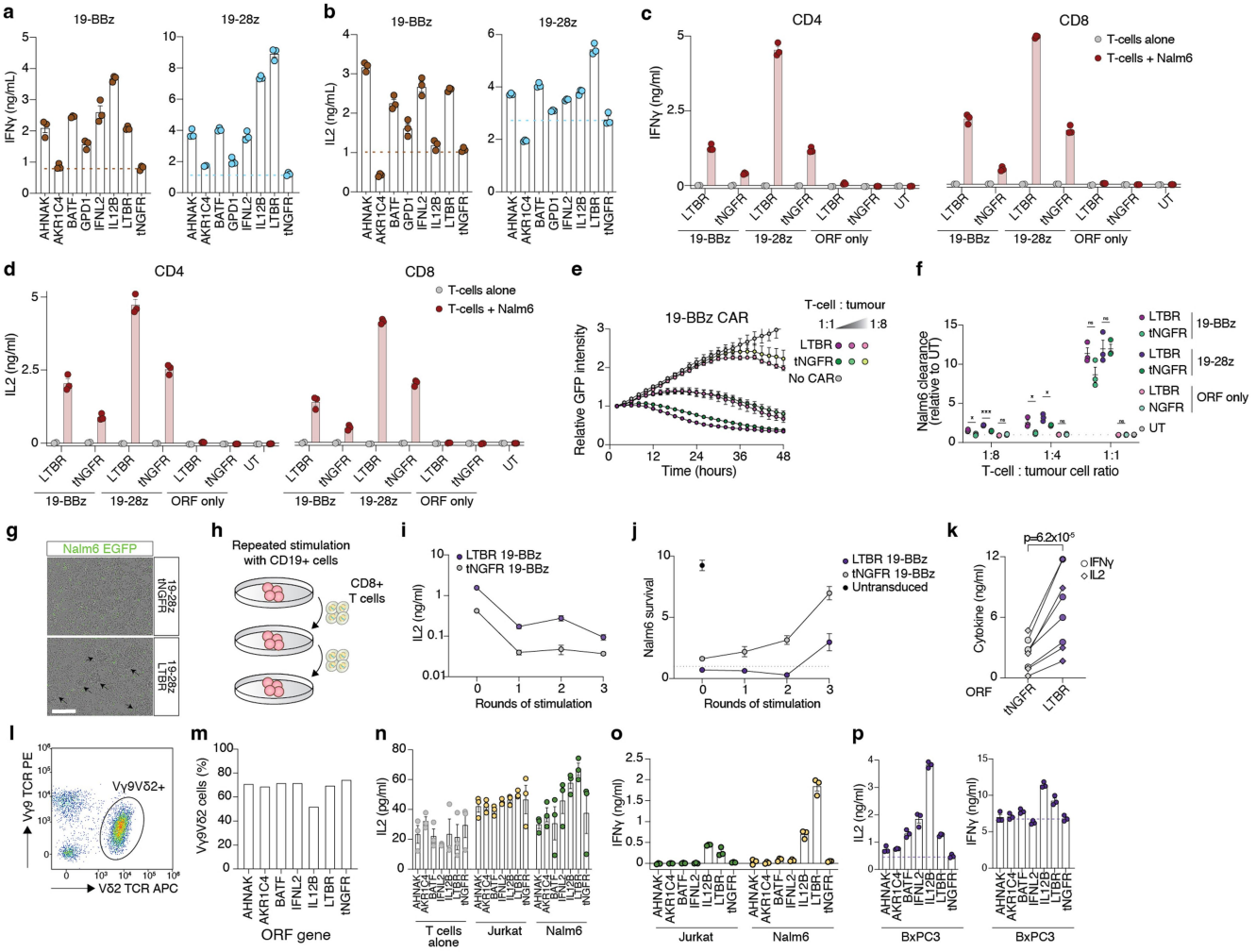

Extended Data Fig. 10 | Top-ranked genes from the ORF screen boost antigen-specific T cell responses. a, **b**, Co-delivery of anti-CD19 CARs and ORFs to T cells from healthy donors. **a**, IFNγ and **b**, IL2 secretion after overnight co-incubation of CD4+ T cells with Nalm6 cells at 1:1 ratio ($n = 3$ biological replicates, representative of two donors). **c**, **d**, IFNγ (**c**) or IL-2 (**d**) secretion by CAR+ORF or ORF only T cells co-incubated for 24 h either alone or with Nalm6 cells. **e**, Cytotoxicity of 19-BBz CAR T cells expressing tNGFR or LTBR ORF after co-incubation with Nalm6 GFP cells. **f**, Quantification of Nalm6 clearance (relative to Nalm6 co-incubated with untransduced T cells) for CAR+ORF or ORF alone T cells at different effector:target ratios. Unpaired two-sided *t*-test *p* values: 0.011, 1.3×10^{-4}, 0.072, 0.02, 0.021, 0.52, 0.087, 1, 0.51 (left to right). **g**, Representative images of T cells transduced with 19-28z CAR and NGFR or LTBR, co-incubated with CD19+ Nalm6 GFP cells for 48 h at 1:1 ratio. Scale bar: 200 µm. **h**–**j**, Repeated stimulation of CAR+ORF T cells with Nalm6 cells. IL-2 secretion (**i**), or Nalm6 survival (**j**), by 19-BBz CAR LTBR or tNGFR T cells re-challenged with Nalm6 after repeated stimulation with Nalm6 cells every three days, for up to three rounds of stimulation. **k**, Secretion of cytokines IL2 and IFNγ by CAR/LTBR or CAR/tNGFR T cells from two patients with DLBCL after overnight incubation with Nalm6 target cells. Two-sided paired *t*-test *p* value is shown. **l**, Representative staining of ORF-transduced T cells endogenously expressing Vγ9Vδ2 TCR. **m**, Quantification of ORF-transduced T cells expressing Vγ9Vδ2 TCR. **n**, **o**, IL2 (**n**) or IFNγ (**o**) secretion after 24 h co-incubation of ORF transduced Vγ9Vδ2 T cells with leukaemia cell lines. **p**, IL2 or IFNγ secretion after 24 h co-incubation of ORF transduced Vγ9Vδ2 T cells with BxPC3, a pancreatic ductal adenocarcinoma cell line. Cell lines in panels **n**–**p** were pre-treated with zoledronic acid prior to co-incubation. Error bars indicate SEM. $N = 3$ biological replicates are shown, unless indicated otherwise.